Climate Dynamics
https://doi.org/10.1007/s00382-018-4171-x

Climate conditions and drought assessment with the Palmer Drought Severity Index in Iran: evaluation of CORDEX South Asia climate projections (2070–2099)

Alfonso Senatore[1] · Somayeh Hejabi[2] · Giuseppe Mendicino[1] · Javad Bazrafshan[2] · Parviz Irannejad[3]

Received: 23 January 2017 / Accepted: 9 March 2018

Abstract
Climate change projections were evaluated over both the whole Iran and six zones having different precipitation regimes considering the CORDEX South Asia dataset, for assessing space–time distribution of drought occurrences in the future period 2070–2099 under RCP4.5 scenario. Initially, the performances of eight available CORDEX South Asia Regional Climate Models (RCMs) were assessed for the baseline period 1970–2005 through the GPCC v.7 precipitation dataset and the CFSR temperature dataset, which were previously selected as the most reliable within a set of five global datasets compared to 41 available synoptic stations. Though the CCLM RCM driven by the MPI-ESM-LR General Circulation Model is in general the most suitable for temperature and, together with the REMO 2009 RCM also driven by MPI-ESM-LR, for precipitation, their performances do not overwhelm other models for every season and zone in which Iranian territory was divided according to a principal component analysis approach. Hence, a weighting approach was tested and adopted to take into account useful information from every RCM in each of the six zones. The models resulting more reliable compared to current climate show a strong precipitation decrease. Weighted average predicts an overall yearly precipitation decrease of about 20%. Temperature projections provide a mean annual increase of 2.4 °C. Future drought scenarios were depicted by means of the self-calibrating version of the Palmer drought severity index (SC-PDSI) model. Weighted average predicts a sharp drying that can be configured as a real shift in mean climate conditions, drastically affecting water resources of the country.

Keywords Palmer Drought Severity Index (PDSI) · Principal components analysis (PCA) · RCMs weighting · RCP4.5 · CCLM · REMO · GPCC v.7 dataset · CFSR dataset

1 Introduction

The Fifth Assessment Report (AR5) of the Intergovernmental Panel on Climate Change (IPCC 2013) confirms the concerns about reduction of water resources availability in a large region extending from Southern Europe to the whole Middle East. In order to better assess the extent and intensity of that projected decrease, several actions are needed, among which the spatial downscaling of the information provided by the General Circulation Models (GCMs) included in the Coupled Model Intercomparison Project Phase 5 (CMIP5; Taylor et al. 2012).

Several authors in the framework of the IPCC Fourth Assessment Report (AR4; IPCC 2007) and CMIP3 performed statistical and dynamical downscaling of climate change scenarios projected by GCMs (Meehl et al. 2007). In particular, Abbaspour et al. (2009) performed an overall

Electronic supplementary material The online version of this article (https://doi.org/10.1007/s00382-018-4171-x) contains supplementary material, which is available to authorized users.

✉ Alfonso Senatore
alfonso.senatore@unical.it

[1] Department of Environmental and Chemical Engineering, University of Calabria, Via P. Bucci 42a, 87036 Rende, CS, Italy

[2] Department of Irrigation and Reclamation, Faculty of Agricultural Engineering and Technology, University of Tehran, Karaj, Iran

[3] Department of Space Physics, Institute of Geophysics, University of Tehran, Tehran, Iran

Published online: 13 March 2018

assessment over Iran. They used the Canadian Global Coupled Model (CGCM 3.1) with a coarse spatial resolution (roughly 2.8°) and, considering the A1B, B1 and A2 GHG emission scenarios (Nakícenovíc et al. 2000), found in general an exacerbation of climate conditions with respect to the baseline period 1980–2002 both in the 2013–2039 and 2073–2099 time slices, with more rainfall over wet regions of the country and less rainfall over dry regions (the latter mainly located in the South-East of the country). After this study, several others followed, mainly focused on specific regions of the country. Using the same GCM and scenarios of Abbaspour et al. (2009), Hashemi et al. (2015) applied a coupled modeling approach to assess climate change impacts on groundwater recharge and management in a Southern arid area, finding no significant differences between present and future recharge for all scenarios. The same GCM and scenarios were used also by Naderi and Raeisi (2016), who focused on a study area with an arid to semiarid climate located in South-Central Iran and applied a statistical downscaling approach, finding temperature increase and annual precipitation decrease during the period 2015–2095. Etemadi et al. (2016) also applied a statistical approach to downscale outputs from two GCMs in an arid South-East coastal region under the A1B scenario, in order to assess climate change impact on the spatial pattern of mangrove ecosystems. Sayari et al. (2013) used some drought indices for assessing climate change impacts under A2 and B2 scenarios in a North-Eastern basin of the country. Adopting a statistical downscaling of HadCM3 outputs, they found a slight increase of average precipitation, but also higher drought frequency associated with global warming along the twenty-first century. Emam et al. (2015), instead, focused on a North-Western catchment. They also used statistical downscaling with four GCMs under A1B, B1 and A2 scenarios, finding a likely decrease of annual precipitation and increase in temperature in the mid-twenty-first century, leading to a substantial reduction in groundwater recharge. Azari et al. (2016) found an increase in annual streamflow for a catchment located in North Iran under A1Fi, B1 and A2 scenarios for 2040–2069. Finally, a dynamical downscaling approach was applied by Solaymani and Gosain (2015) over a basin in the south-west of the country, finding a considerable reduction in water yield mainly in the summer period, due to the increase in average temperature and decrease in precipitation.

To the knowledge of the authors, so far only Kouhestani et al. (2016) published a study on GCMs outputs from the newest version of the Fifth Assessment Report (AR5) specifically focused on wide Iranian areas. They performed an analysis over one of the main basins in central Iran using fifteen GCMs from CMIP5 multi-model ensemble regridded at $2.5° \times 2.5°$, finding a reduction of precipitation in most of the basin both at near-term (2015–2050) and long-term (2015–2100), considering both RCP2.6, RCP4.5 and RCP8.5 radiative forcing scenarios (Moss et al. 2010).

In order to aid climate change impact and adaptation studies within the timeline of the AR5 and beyond, the Coordinated Regional Downscaling Experiment (CORDEX) program (Giorgi et al. 2009) was established, providing a common experiment protocol for generating large ensembles of climate projections based on regional climate downscaling techniques over regions worldwide. So far, CORDEX is the biggest effort of the scientific community for enabling the transfer of know-how across regional settings (Giorgi and Gutowsky 2016).

More than one CORDEX domain contains the whole territory of Iran. The most adequate for studying climate change projections are Region 6 (South Asia) and Region 13 (Middle East North Africa—MENA), where Iran is well within the domains borders. Concerning the MENA-CORDEX Program, so far the main published outputs relates to parameterization issues (Bucchignani et al. 2016a, b; Almazroui et al. 2016; Almazroui 2016; Zittis et al. 2014), even though RCPs scenarios simulations are becoming increasingly available. However, Terink et al. (2013) already performed climate change projections for the MENA region before the MENA-CORDEX domain was established, using climate data from the CMIP3 model ensemble and the A1B scenario. They found especially for central and eastern Iran large precipitation decreases (up to 20%) up to 2050. Concerning CORDEX South Asia, together with publications involved with parameterization issues or performance evaluation (especially concerning summer monsoon features, e.g., Raju et al. 2015; Ghimire et al. 2015), some climate projections results are becoming available and are related also to hydrological impact (Li et al. 2016; Pechlivanidis et al. 2016), but they focus especially on the Indian subcontinent. Even though their work still refers mainly to India, Dash et al. (2015) provided some information about projected seasonal mean summer (from June to September) monsoon also for the adjoining regions, using the regional model RegCM4 (Giorgi et al. 2012). For Iran, some precipitation increase is projected in the southern coast under both RCP4.5 and RCP8.5 scenarios from the near (2010–2039) to the far (2070–2099) future.

The Phase I CORDEX RegCM hyper-Matrix (CREMA; Giorgi 2014) provides a series of experiments over different CORDEX domains, among which the South Asia domain, performed by the network of RegCM users worldwide. In the framework of the CREMA experiment, some results specifically concerning average temperature and precipitation changes in Iran can be inferred from Coppola et al. (2014). Considering RegCM simulations for the period 2070–2099 with respect to 1976–2005 reference period, a rather homogeneous mean annual ensemble temperature increase of up to 6 °C under RCP8.5 scenario

was found. Detected precipitation changes were much less uniform, but generally, under RCP8.5 scenario a slight increase was predicted. Giorgi et al. (2014), on the other side, predicted under the same RCP scenario and for the same time period a generally high increase in the maximum number of consecutive dry days (up to 75 in central Iran). However, in their results some spatial inconsistencies appear because Iran was subdivided among different CREMA domains, and the Iranian areas depending on the Mediterranean domain were much drier than the others.

In the present study, the simulations performed over South Asia Region were chosen for assessing climate change scenarios in Iran, leaving out for future developments a similar analysis with the CORDEX simulations over the MENA region. The main objective is to address the need for downscaling information to a resolution fitting to the regional scale and to provide projections of climate change impact on monthly precipitation, temperature and drought conditions assessed through the self-calibrating version of the Palmer Drought Severity Index (SC-PDSI; Palmer 1965; Wells et al. 2004). To this aim, eight Regional Climate Models (RCMs) available from the CORDEX South-Asia experiment were used for dynamical downscaling, assessing both their performance with the baseline period 1970–2005 and their projections for the future period 2070–2099 under RCP4.5 scenario. Specifically, the paper is organized with three sections besides this Introduction. Section 2 is subdivided in several subsections and describes the procedures for selecting the most trustworthy monthly temperature and precipitation datasets to be used as references for the investigation of the reliability of CORDEX South-Asia RCMs, outlines the RCMs used and their properties, depicts the weighting scheme selected for combining the model ensemble output in order to retain as much information as possible, even by the least performing models, and provides methodological details about the use of the SC-PDSI for future scenarios; Sect. 3 shows the main results concerning analysis and reanalysis datasets reliability, RCMs performances with the baseline period and climate change projections; finally, in Sect. 4 conclusions of the paper are drafted.

2 Study area, data and analysis methods

2.1 Observational, analysis and reanalysis datasets

The high spatial and temporal variability of precipitation over Iran, the shortness of climatological records at most stations, the sparse distribution of stations with the longest records across the country and 3–5 years delays in publishing the updated data by the Iranian Meteorological Organization are the most important limitations for studying drought monitoring in Iran (Raziei et al. 2011). A contribution to the solution of this problem may be given by global gridded analysis and reanalysis datasets. Therefore, monthly temperature and precipitation data investigated in this study were obtained from three sources: (1) Observation records of synoptic stations, (2) Global high resolution gridded analysis datasets and (3) Global high resolution gridded reanalysis datasets.

Raw precipitation and temperature data were achieved from monthly observations recorded at 41 synoptic stations whose historical records cover the period 1970–2005 (Table S1 in supplementary material). Among the global high resolution analysis datasets, Global Precipitation Climatology Centre (GPCC) Full Data Product Version 7 (Schneider et al. 2015) and Climatic Research Unit Time-Series (CRU-TS) Version 3.23 (Harris et al. 2014) datasets were selected for this study. In addition, among the global atmospheric reanalysis datasets, European Centre for Medium-Range Weather Forecasts (ECMWF) ERA-Interim (Dee et al. 2011), ECMWF Atmospheric Reanalysis of the twentieth Century (ERA-20C; Poli et al. 2016) and the National Centers for Environmental Prediction (NCEP) Climate Forecast System Reanalysis (CFSR; Saha et al. 2010) datasets were used. Except GPCC v.7 dataset, which provides only precipitation data, the other datasets contain both precipitation and temperature data. More details about all datasets are provided in Table 1, while Fig. 1 shows the location of the synoptic stations, and grid points of the analysis and reanalysis datasets over Iran. For compatibility of all datasets, a spatial resolution of 0.5°×0.5° latitude by longitude was chosen for both monthly temperature and precipitation variables. Except the ERA-Interim and CFSR datasets, which

Table 1 Details of datasets applied in this study

Dataset type	Dataset name	Spatial coverage	Temporal coverage	Variable
Analysis	GPCC v.7	179.75W–179.75E, 89.75S–89.75N	1901–2013	Precipitation
	CRU-TS v. 3.23	179.75W–179.75E, 89.75S–89.75N, all land areas (excluding Antarctica)	1901–2014	Precipitation, temperature
Reanalysis	ERA-Interim	180W–180E, 90S–90N	1979–2013	Precipitation, temperature
	ERA-20C	180W–180E, 90S–90N	1900–2010	Precipitation, temperature
	CFSR	180W–180E, 90S–90N	1979–2011	Precipitation, temperature

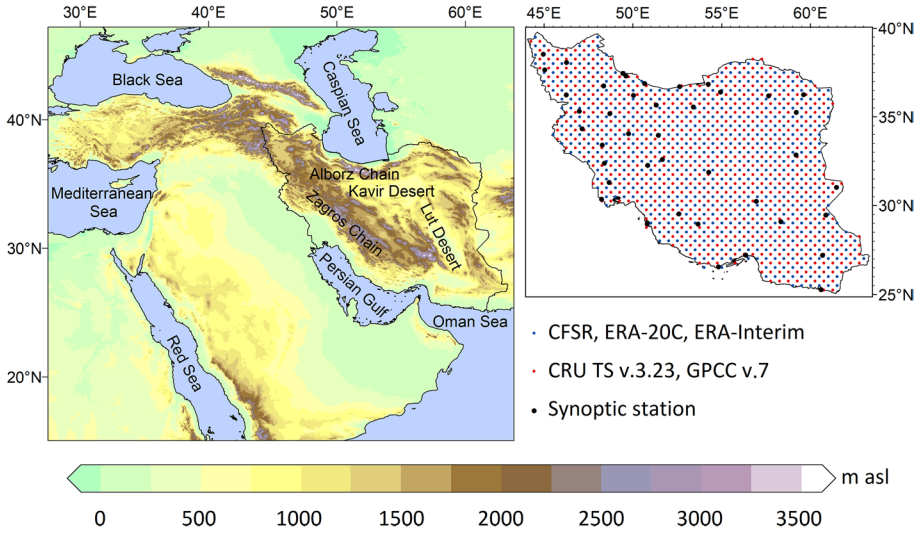

Fig. 1 Location and topography of Iran (left) and synoptic stations and grid points of the analysis and reanalysis datasets over Iran (right)

are available from 1979 to 2005, the evaluation period for other datasets covers the years from 1970 to 2005.

Statistical comparisons were performed for each synoptic station with the closest grid point of each dataset to the station coordinates. The period covered by GPCC v.7, CRU-TS v.3.23 and ERA-20C was 1970–2005, while it was 1979–2005 for ERA-Interim and CFSR. Agreement between the long term average of monthly precipitation and temperature provided by the synoptic stations and each dataset was evaluated by means of scatter plots. Also, different performance indicators including correlation coefficient, root mean square error (RMSE) and bias were used for evaluating seasonal precipitation and temperature gridded datasets.

2.2 Principal component analysis

With the aim of assessing the reliability of the analysis and reanalysis datasets of monthly precipitation over specific climatic regions of Iran, a precipitation-based regionalization was performed using the Principal Component Analysis (PCA; Rencher 1998) with varimax rotation. The varimax orthogonal rotation, as a commonly used rotational method for meteorological map typing, was used for rotating a predetermined number of PCs toward simple structure. The number of components retained for rotation were determined by means of the Scree test (Cattel 1966) and the North rule of thumb (North et al. 1982). The interpretation given by North et al. (1982) is that "... if a group of true eigenvalues (λ) lie within one or two $\delta\lambda$ [eigenvalue standard error] of each other then they form an 'effectively degenerate multiplex', and sample eigenvectors are a random mixture of the true eigenvectors". The first guess of eigenvalues standard error can be estimated by the Lawley's formula (Lawley 1956):

$$\delta\lambda \approx \lambda\left(\frac{2}{N}\right)^{0.5} \quad (1)$$

where N is the sample size and λ is an eigenvalue.

Once the eigenvalues, λ_i, have been computed, the spacing between them, λ_{i+1}-λ_i, is calculated. Using Eq. (1), an estimate of the standard error is determined and those eigenvalues which lie within confidence intervals of error are noted.

The retained components were rotated using varimax method to find better localized spatial patterns of variability. Following Raziei (2017), the maximum loading value approach was then used for precipitation regionalization. This approach is based on assigning each station (grid point) to a component upon which it loads most highly. The Kolmogorov–Smirnov (K-S) test was used for testing the homogeneity of the identified zones. The evaluation of the most reliable analysis/reanalysis dataset reproductions was finally performed for each zone.

2.3 CORDEX South Asia regional climate model experiments

The investigation of the reliability of CORDEX South-Asia RCMs against observed data was performed using grid-based comparison of the selected analysis/reanalysis datasets of precipitation and temperature with gridded CORDEX South-Asia RCMs data.

In this study, we applied the simulations from eight CORDEX South Asia RCMs experiments at 0.44° resolution which are different combinations of six GCMs and four RCMs (namely CCAM, McGregor and Dix 2001; REMO 2009; Rechid et al. 2009; RCA4; Samuelsson et al. 2011; CCLM4; Dobler and Ahrens 2008). Table 2 shows the list of CORDEX South Asia RCMs experiments (updated information about CORDEX-South Asia Datasets is available at http://cccr.tropmet.res.in/home/ftp_data.jsp). In the first five experiments, the same RCM (i.e. CCAM) was run with

Table 2 List of CORDEX South Asia regional climate model (RCM) experiments

Experiment abbreviation	Driving GCM	RCM	Contributing institute
AC-CCAM	ACCESS1.0	CCAM	CSIRO Marine and Atmospheric Research, Melbourne, Australia
CC-CCAM	CCSM4		
CN-CCAM	CNRM-CM5		
MP-CCAM	MPI-ESM-LR		
NO-CCAM	NorESM-M		
MP-REMO	MPI-ESM-LR	REMO 2009	Climate Service Center, Hamburg, Germany
EC-RCA4	EC-EARTH	RCA4	Rossy Centre, Swedish Meteorological and Hydrological Institute (SMHI), Sweden
MP-CCLM	MPI-ESM-LR	CCLM4	Institute for Atmospheric and Environmental Sciences (IAES), Goethe University, Frankfurt am Main (GUF), Germany

boundary forcing from five different GCMs. In the cases of the three experiments MP-CCAM, MP-REMO and MP-CCLM, three different RCMs were run with the boundary forcing from the same GCM (i.e. MPI-ESM-LR). Therefore, this study focuses on differences among the results of several combinations of GCMs and RCMs, representing a significant source of uncertainty. Nevertheless, it is noteworthy to highlight that also other sources of uncertainty should be taken into account in order to provide a more comprehensive picture, such as, e.g., the effects of different physical parameterizations (Juneng et al. 2016; Ngo-Duc et al. 2017).

After regridding the datasets to the same domain and resolution ($0.5° \times 0.5°$ latitude by longitude), the reliability of CORDEX South Asia RCMs was evaluated against the most reliable analysis/reanalysis dataset for the historical period from 1970 to 2005. Visual evaluation of long-term average of simulated monthly precipitation/temperatures against the most reliable analysis/reanalysis dataset was initially performed using scatter plots. Then, at the seasonal scale, performance indicators (correlation coefficient, RMSE, bias) were used for comparing precipitation/temperature of each CORDEX South Asia RCM with the most reliable analysis/reanalysis dataset. In addition, monthly precipitation/temperature regimes from the CORDEX South Asia RCMs dataset in each climatic zone were compared with their corresponding values from the most reliable analysis/reanalysis dataset.

2.4 Weighting procedure and climate change impact analysis

In the perspective of future climate assessment, a way to reduce the uncertainty of the modeling ensemble when dealing with numerous climate change projections can be a weighting approach, where the weighting is based on single models performances (Christensen et al. 2010). Several methods are available (e.g. Giorgi and Mearns 2002; Räisänen et al. 2010; Räisänen and Ylhäisi 2012; Boé and Terray 2015), some of which were also applied in Iran (Rahmani and Zarghami 2013; Zareian et al. 2015). In this study, for computing the ensemble mean values of the RCMs simulations, in addition to simple averaging of them, the robust yet simple model-weighting approach proposed by Coppola et al. (2010) was applied. This approach is based on five performance indicators:

$$g_1 = R\left(P_{RCM}, P_{grid}\right) \tag{2}$$

$$g_2 = R\left(T_{RCM}, T_{grid}\right) \tag{3}$$

$$g_3 = \sigma(P_{grid})/RMSE(P) \tag{4}$$

$$g_4 = \sigma(T_{grid})/RMSE(T) \tag{5}$$

$$g_5 = \left[1 - \frac{\left|R\left(P_{grid}, T_{grid}\right) - R\left(P_{RCM}, T_{RCM}\right)\right|}{2}\right] \tag{6}$$

where P and T represent seasonally averaged precipitation and temperature, respectively; subscripts $_{\mathrm{RCM}}$ and $_{\mathrm{grid}}$ represent CORDEX South Asia RCM and the most reliable analysis/reanalysis dataset, respectively; R is the spatial correlation coefficient between observed and simulated mean values calculated for each season and over a region of interest; RMSE represents the Root Mean Square Error; and σ is a measure of the interannual variability of the observed mesoscale signal. To obtain σ, the mean values were first calculated at each grid point for every season of each year of the selected time period. This time series of seasonal values was then used to compute the interannual standard deviation at each grid point, which was then averaged over all the grid points in the domain of interest to yield σ. g_5 is the spatial correlation between precipitation and temperature. Note that the performance indicators are

all normalized to yield non-dimensional values between 0 and 1 and also, each performance indicator was calculated separately for the 4 seasons: December–January–February (DJF), March–April–May (MAM), June–July–August (JJA) and September–October–November (SON). The joint time period of the most reliable analysis/reanalysis datasets of precipitation and temperature within historical period was considered for computing the performance indicators. The weight for each RCM is given by:

$$w_i = g_1^{j1} \times g_2^{j2} \times g_3^{j3} \times g_4^{j4} \times g_5^{j5} \quad (7)$$

where w_i is the weight for ith RCM, and the exponents j can be used to differentiate impacts of the performance indicators. From these weights, the weighted mean value of a variable (temperature or precipitation) obtained from the ensemble of models is given by:

$$\bar{X} = \frac{\sum_i w_i X_i}{\sum_i w_i} \quad (8)$$

where X_i is the value of the variable (temperature or precipitation) for RCM i.

In order to explore the best combinations of performance indicators, following Coppola et al. (2010) we tested five cases of different combinations of g_1–g_5 as described in Table 3. In Combination 1, all the g_1–g_5 functions are used; in Combination 2, the function g_5 is removed; and in Combination 3, functions g_1 and g_2 provide more contribution to the weight than the others. In Combination 4 and 5, only precipitation-based or temperature-based performance indicators are applied. Performance of the different combinations was investigated through a statistical comparison of the seasonal time series of weighted means of the variables with those of the most reliable analysis/reanalysis datasets.

Concerning climate change impact analysis, the selected future projections of precipitation and temperature in CORDEX South Asia RCMs are based on RCP4.5 scenario and cover the period from 2070 to 2099. The comparison of future precipitation and temperature projections with the historical period was performed through calculating the ratios (differences) of precipitation (temperature) projections vs. their historical values at seasonal and annual time scales.

Table 3 Different performance indicators combination

Number	Performance indicators combination
1	$g_1 \times g_2 \times g_3 \times g_4 \times g_5$
2	$g_1 \times g_2 \times g_3 \times g_4$
3	$g_1^{0.5} \times g_2^{0.5} \times g_3 \times g_4$
4	$g_1 \times g_3$
5	$g_2 \times g_4$

All comparisons were performed for both the whole Iran and each zone separately. Moreover, weights of RCMs from the selected (i.e. the more performing) combination of performance indicators were applied to calculate the weighted averages of future projections for the analyzed variable (temperature or precipitation).

2.5 The self-calibrating Palmer Drought Severity Index

In order to compare future drought events with the historical period, drought was quantified with the SC-PDSI forced with weighted averages of monthly precipitation and temperature data. SC-PDSI automatically calibrates the behavior of the index at any location by replacing empirical constants in the index computation with dynamically calculated values (Wells et al. 2004). The PDSI bucket model uses the Thornthwaite algorithm (Thornthwaite 1948) for potential evapotranspiration, which is solely a function of air temperature, therefore implicitly assumes a uniform surface (Van der Schrier et al. 2011).

The historical period was considered as the reference period for calibrating the SC-PDSI parameters. Water-holding capacity data was obtained from a soil texture–based water-holding-capacity map produced by Webb et al. (2000). The SC-PDSI values for the future time slice (2070–2099) were calculated based on the future projections of precipitation and temperature from the eight available RCMs of CORDEX South Asia. The evaluation of historical vs. future SC-PDSI values was performed by comparing the spatial pattern of long term SC-PDSI average over Iran and investigating the projected changes in the SC-PDSI histogram.

3 Results

3.1 Datasets evaluation results

Figure 2 shows the values of the long term monthly mean precipitation of the grid points from the analysis and reanalysis datasets against those observed at the closest synoptic stations, while Fig. 3 shows similar plots for temperature. Points distribution on the scatter plots, slope and intercept of the regression lines together with the coefficient of determination (R^2) indicate that GPCC v.7 dataset presents the best estimation of long term monthly mean precipitation (Fig. 2), while CFSR dataset represents better monthly temperature (even though it has to be noted that in the temperature comparison, unlike precipitation, statistical measures are not very different among the four datasets).

Efficiency of analysis/reanalysis datasets in estimating the mean seasonal precipitation and temperature was evaluated also by calculating correlation coefficient, root mean

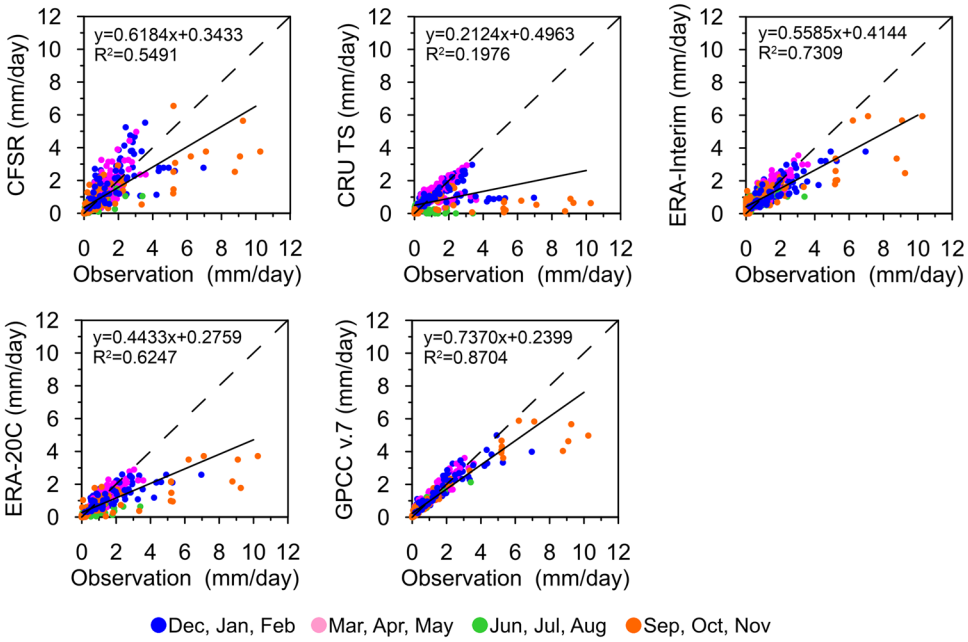

Fig. 2 Comparison of long term average of monthly precipitation at 41 stations with corresponding values of the closest grid points from analysis and reanalysis datasets

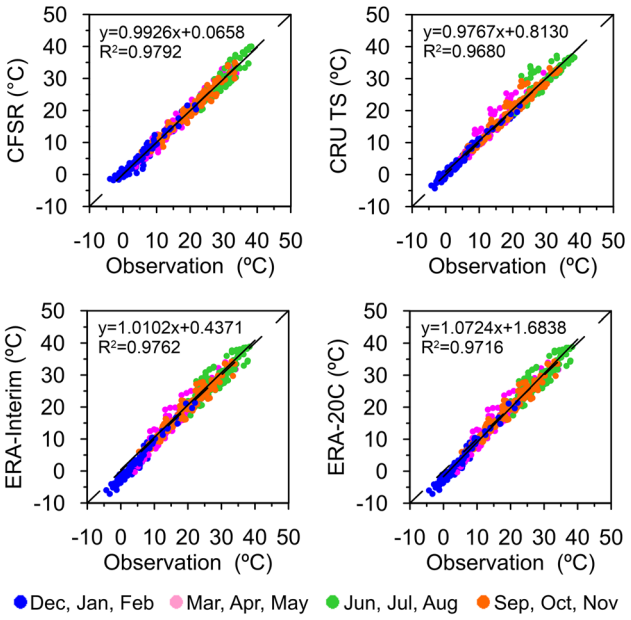

Fig. 3 Comparison of long term average of monthly temperature at 41 stations with corresponding values of the closest grid points from analysis and reanalysis datasets

square error (RMSE) and bias (Tables 4, 5). Table 4 shows the superiority of GPCC v.7 for seasonal precipitation, with JJA having the highest consistency with the observations (r = 0.95, RMSE = 0.20, bias = 0.00). Concerning temperature, strong correlations (higher than 0.9) between gridded and station data (Table 5) suggest that all datasets capture the spatial pattern of temperature fairly well. However, the bias values of CFSR in winter, spring and autumn are very small in comparison with the other three datasets and, despite the higher summer bias of CFSR in comparison with CRU TS v.3.23 and ERA-20C, its RMSE is by far the lowest. Altogether, the CFSR dataset was selected as the most reliable dataset for temperature, based on its higher efficiency in simulating both the long term monthly and seasonal temperature.

In order to capture the patterns of variability of monthly precipitation and temperature at different stations/grid points, the PCA was applied to the simulated and observed monthly precipitation and temperature data. The spatial patterns of loadings were obtained by interpolating the loading values using inverse distance weighting (IDW) method. Because of unavailability of ERA-Interim and CFSR

Table 4 Correlation coefficient, root mean square errors and bias between seasonal precipitation at 41 stations with corresponding values of the closest grid points from analysis and reanalysis datasets

Dataset	Correlation coefficient				RMSE (mm/day)				Bias (mm/day)			
	DJF	MAM	JJA	SON	DJF	MAM	JJA	SON	DJF	MAM	JJA	SON
GPCC v.7	0.91	0.93	0.95	0.94	0.58	0.32	0.20	0.93	−0.02	0.10	0.00	−0.17
CRU TS v.3.23	0.51	0.75	0.06	0.29	1.24	0.55	0.63	2.13	−0.39	−0.01	−0.10	−0.61
ERA-20C	0.71	0.79	0.62	0.79	1.06	0.51	0.51	1.64	−0.38	−0.08	−0.15	−0.48
ERA-Interim	0.76	0.80	0.50	0.84	0.90	0.53	0.54	1.32	−0.24	0.09	0.21	−0.13
CFSR	0.64	0.66	0.71	0.80	1.14	0.78	0.41	1.44	0.15	0.13	−0.09	−0.31

Table 5 Correlation coefficient, root mean square errors and bias between seasonal temperature at 41 stations with corresponding values of the closest grid points from analysis and reanalysis datasets

Dataset	Correlation coefficient				RMSE (°C)				Bias (°C)			
	DJF	MAM	JJA	SON	DJF	MAM	JJA	SON	DJF	MAM	JJA	SON
CRU TS v.3.23	0.99	0.93	0.80	0.94	1.12	2.08	2.68	1.80	0.31	0.43	0.39	0.43
ERA-20C	0.97	0.93	0.85	0.93	2.31	2.23	2.48	1.88	−1.53	−0.30	0.31	−0.01
ERA-interim	0.97	0.95	0.91	0.96	1.54	2.08	2.15	1.72	0.46	0.49	0.72	1.03
CFSR	0.97	0.97	0.93	0.96	1.55	1.50	1.86	1.46	0.06	0.08	−0.40	−0.02

datasets for the period 1970–1978, the PCA method for observations was also performed for the period 1979–2005 in addition to 1970–2005. However, since no significant differences in the percentages of the explained variance, rotated PC score time series and loading patterns were observed, results of PCA method for observations are reported only for the period 1970–2005. In the case of precipitation, five components were selected as the final number of components to retain for varimax rotation for observations. Instead, six components for GPCC v.7, CRU TS v3.23 and ERA-Interim, four for ERA-20C and five for CFSR were retained, respectively. Table 6 shows the percentages of the variance explained by the selected PCs for the observed and the gridded datasets of precipitation. Rotated loadings patterns of monthly precipitation for observed, analysis and reanalysis datasets are shown in Fig. 4. It must be noted that loadings represent the correlation between observation time series and associated PC scores.

Comparison of the rotated loading patterns of observed and simulated monthly precipitation reveals that rotated loading patterns of GPCC v.7 agree more with observed. Specifically, the GPCC v.7 is the only dataset that captures well the pattern of the rotated loading of Caspian Sea coastal areas.

Correlation coefficients between rotated PC time series of observed and simulated monthly precipitation are listed in Table 7. Correlation values related to the loadings of analysis/reanalysis datasets that in Fig. 4 were associated to specific observation loadings are shown in bold (e.g. PC1 for observations and PC4 for GPCC v.7). Table 7 highlights that altogether, rotated PC scores of GPCC v.7 data are in good agreement with those of observed precipitation data. Furthermore, it was found that both the first and fifth PCs of GPCC v.7 are correlated with the fourth PC of observations. Thus, the fourth rotated loading pattern of observations was identified with two different PCs in GPCC v.7. This difference can be related to the simultaneous effects of the Sudan thermal lows and Mediterranean frontal systems in this region, which was not detected by the available low-density station network.

Results of PCA method for monthly temperature revealed that the percentages of the total variance explained by the first PC for CRU TS v.3.23, ERA-Interim, ERA-20C, CFSR and observations are 98.49, 98.34, 98.35, 98.12 and 97.21% respectively. Therefore, the first PC explains almost all the variance of monthly temperature data. The first rotated loading of the observed and monthly temperature is characterized by high positive values (close to 1) all over Iran (not shown).

The rotated loading patterns can be used for establishing a regional zoning. This exercise was already performed for Iran by several authors (Domroes et al. 1998; Dinpashoh et al. 2004; Modarres and Sarhadi 2011; Sarmadi and Shokoohi 2015; Raziei et al. 2012; Raziei 2017). Because of the similarity of spatial and temporal patterns of temperature in all stations/grid points, zoning process was performed only based on precipitation. Even though, based on observations, five spatial zones were found (this is consistent with the findings of Raziei et al. 2012 and; Raziei 2017), precipitation regionalization based on GPCC v.7 identifies six spatial zones (Fig. 5), dividing the fourth zone found with observations in two further zones. Thus, since following analysis is not based on observations, but on the most reliable analysis/reanalysis precipitation and

Table 6 Percentages of the explained variances of un-rotated (UR) and varimax rotated (R) PCs for observed, analysis and reanalysis datasets of monthly precipitation

PC	Observations		GPCC v.7		CRU-TS v.3.23		ERA-Interim		ERA-20C		CFSR	
	UR	R	UR	R	UR	R	UR	R	UR	R	UR	R
PC1	46.16	21.00	56.40	22.34	59.17	15.90	48.20	15.07	64.51	26.22	58.43	18.41
PC2	10.43	17.63	11.04	14.47	10.73	16.94	13.84	14.21	12.86	20.12	9.42	18.79
PC3	7.87	8.31	4.35	11.32	4.03	15.25	6.61	12.86	4.68	21.67	4.18	11.76
PC4	4.17	14.45	3.84	15.57	3.64	10.16	5.08	13.46	4.09	18.13	4.10	16.63
PC5	3.18	10.42	2.40	13.91	2.69	13.67	4.12	16.05			2.60	13.14
PC6			2.16	2.58	2.49	10.84	2.97	9.17				
Total	71.81	71.81	80.19	80.19	82.76	82.76	80.82	80.82	86.14	86.14	78.72	78.72

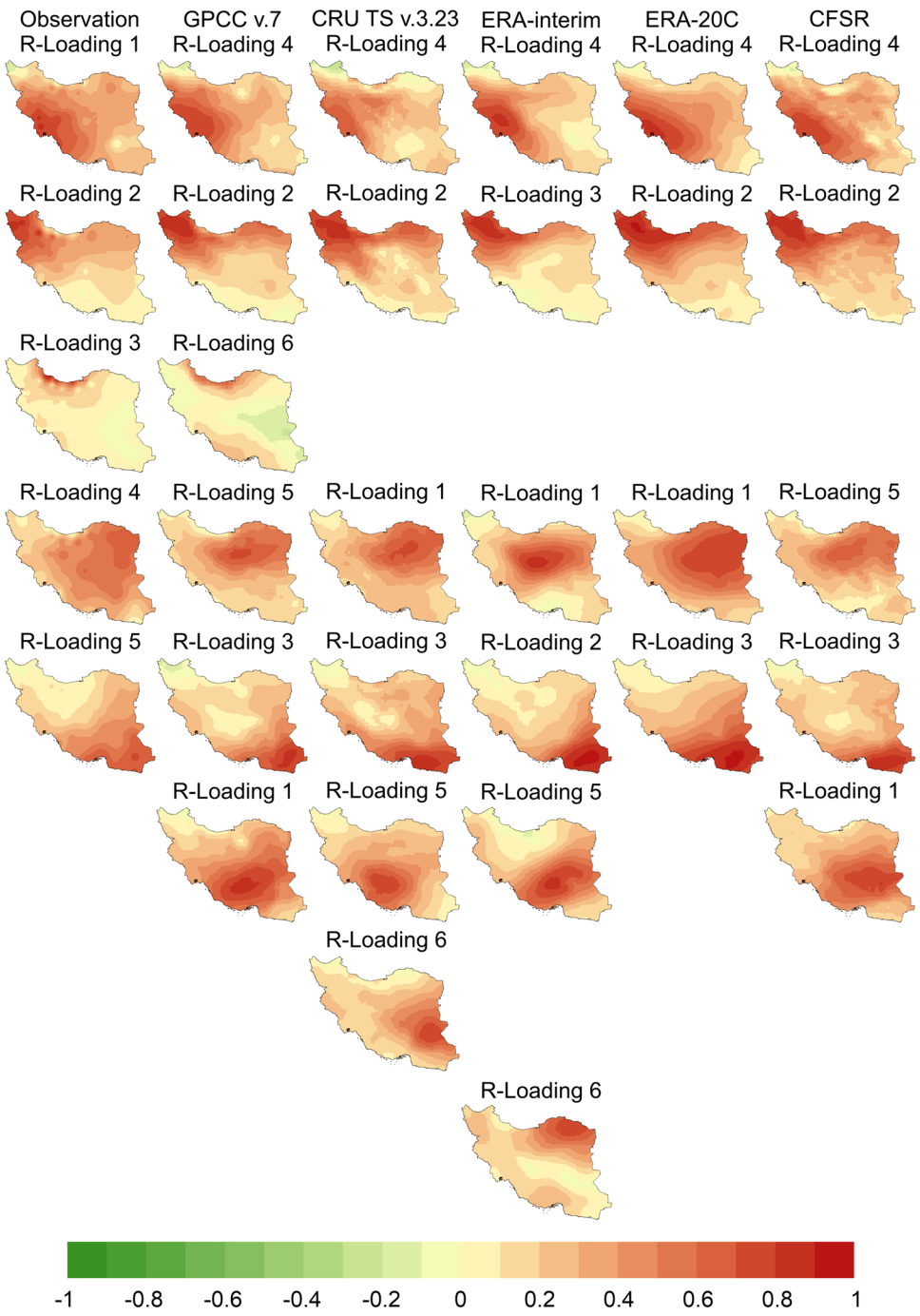

Fig. 4 Rotated loadings of monthly precipitation for observed, analysis and reanalysis datasets

temperature datasets, we fixed six zones. The numbering of the zones in Fig. 5 is identical with the GPCC v.7 loadings numbers. Each zone is representative of a different precipitation regime.

In order to allow a visual comparison of the seasonal pattern of observed precipitation in each climate zone with GPCC v.7, the percentage of annual precipitation for each month was derived from long term observed and reproduced monthly precipitation and averaged over all the stations (or closest grid points) associated with each zone. In addition, statistical comparison of observed and reproduced seasonal precipitation time series was performed using several performance indicators. The results, highlighting for each zone reasonable results, are shown in supplementary material (Figure S1 and Table S2).

3.2 RCMs performance with the baseline period

RCMs performance results are based on simulations performed at the resolution available for our study in the

Table 7 Correlation coefficients between the rotated PCs for observed, analysis and reanalysis datasets of monthly precipitation

		Observation				
	PC	PC1	PC2	PC3	PC4	PC5
GPCC v.7	PC1	0.24	−0.15	0.01	**0.53**	0.40
	PC2	−0.09	**0.93**	0.11	0.12	0.01
	PC3	0.06	0.03	−0.01	−0.05	**0.80**
	PC4	**0.90**	0.15	0.08	−0.13	−0.09
	PC5	0.08	0.08	−0.10	**0.70**	−0.11
	PC6	0.07	−0.07	**0.67**	−0.01	−0.01
CRU TS v.3.23	PC1	0.13	0.03	0.00	**0.68**	−0.08
	PC2	−0.02	**0.92**	0.04	0.12	−0.06
	PC3	0.18	0.01	0.07	−0.05	**0.81**
	PC4	**0.80**	0.12	0.16	−0.15	−0.11
	PC5	0.37	−0.13	−0.01	0.34	0.11
	PC6	−0.06	0.05	−0.15	0.42	0.34
ERA-Interim	PC1	0.05	0.13	−0.01	**−0.01**	0.26
	PC2	0.08	−0.07	0.06	0.17	**0.01**
	PC3	0.06	**0.36**	0.02	0.17	0.01
	PC4	**0.33**	0.00	0.05	0.03	0.08
	PC5	0.13	0.03	−0.01	0.13	0.28
	PC6	0.10	0.25	−0.10	0.18	0.07
ERA-20C	PC1	0.13	0.03	−0.07	**0.72**	0.09
	PC2	0.14	**0.83**	0.18	0.13	−0.03
	PC3	0.10	−0.03	0.06	0.06	**0.78**
	PC4	**0.75**	−0.04	0.01	0.03	0.06
CFSR	PC1	0.09	0.09	−0.02	0.07	0.32
	PC2	0.18	**0.47**	0.03	0.18	0.07
	PC3	0.11	−0.06	0.03	0.21	**0.02**
	PC4	**0.40**	−0.07	0.09	0.04	0.14
	PC5	0.04	0.12	−0.14	**0.18**	0.16

Correlation coefficients between rotated PCs associated to the same zones (Fig. 4) are shown in bold

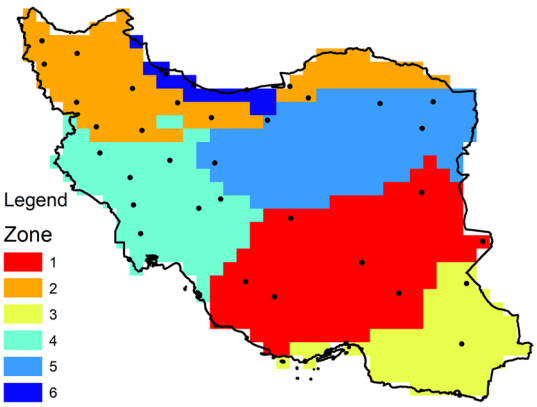

Fig. 5 The homogenous climate zones of Iran derived from principal component analysis of monthly precipitation

CORDEX South Asia dataset, i.e. 0.44° that is higher than 0.5° resolution of the GPCC dataset used for comparison with observations. For some CORDEX domains, resolutions up to 0.11° are available, however higher resolution does not necessarily mean greater accuracy. Improving resolution from 0.44° to 0.22° in the MENA domain, Bucchignani et al. (2016a) found modest enhancements, ascribing their results mainly to the inadequacy of some of the physical schemes adopted. Also Kotlarski et al. (2014) in their EURO-CORDEX standard evaluation paper did not find relevant improvements refining resolution from 0.44° to 0.22°. To the contrary, Prein et al. (2016) using more detailed observational datasets found consistent improvements, in terms of both reduction of seasonal biases and seasonal mean spatial patterns of (especially high) precipitation. However, all these analyses were performed with hindcast simulations (mainly forced by ERA-Interim reanalysis), i.e. without evaluating the relative weight of both errors induced by reduced resolution and GCMs simulations. Using EURO-CORDEX data for climate change projections in the Alps, Smiatek et al. (2016) found that, despite the higher model resolution with respect to previous experiments, simulations with a resolution of 0.11° still revealed substantial biases in

the complex Alpine terrain. Based on previous experience, it is therefore expected that 0.44° resolution can provide a sufficiently accurate picture of the main climate change features in an area as large as Iran.

The first evaluation of the CORDEX South Asia RCMs performance with the baseline period 1970–2005 concerned the pixel-by-pixel comparison with the observational datasets of the long-term average values of the variables needed for PDSI calculation. Figures 6 and 7 show the scatter plots of the RCMs vs. respectively GPCC v.7 monthly precipitation and CFSR monthly average temperature, divided by season. Specifically, Fig. 6 shows that the most suitable RCMs are MP-REMO and MP-CCLM followed by EC-RCA4, while all the CCAM simulations perform worse. All RCMs underestimate GPCC v.7 values, even though summer and autumn precipitation in general are overestimated. Table 8 shows detailed values of the correlation coefficient, RMSE and bias for each model aggregated by season (we preferred to show seasonally aggregated rather than monthly results for the sake of conciseness and clarity, achieving no significant loss of information). Focusing on the MPI-ESM-LR-driven RCMs, significant differences were observed between REMO, CCLM and, mainly, CCAM, highlighting the role of the structural uncertainty of the RCMs in dynamical downscaling. An analogous comparison between the host GCM and GPCC v.7 monthly precipitation (regridded at the GCM resolution, i.e., about 1.87°) is also shown in both Fig. 6 (bottom-right graph) and Table 8, highlighting the added value that can be provided by the RCM experiments in terms not only of spatial resolution but also of accuracy. The most fitting model in winter and spring is MP-REMO, even though for these seasons MP-CCLM provides lower biases. The latter model is the best in summer and autumn, even though in this latter season the lowest bias is provided by MP-REMO.

Comparisons of the temperature variable, which is much less subject to internal variability than precipitation (Hingray and Saïd 2014; Fatichi et al. 2016), led to much more reliable results for all RCMs. Figure 7 shows that the slopes of the scatterplots are in the range 0.90–1.01. The main difference is the scattering around the 1:1 line. Again, the CCAM simulations provide worse results. Detailed statistics by season and model (Table 9) show that the most performing model is MP-CCLM for almost each statistic and season. Interestingly, CCAM models always overestimate

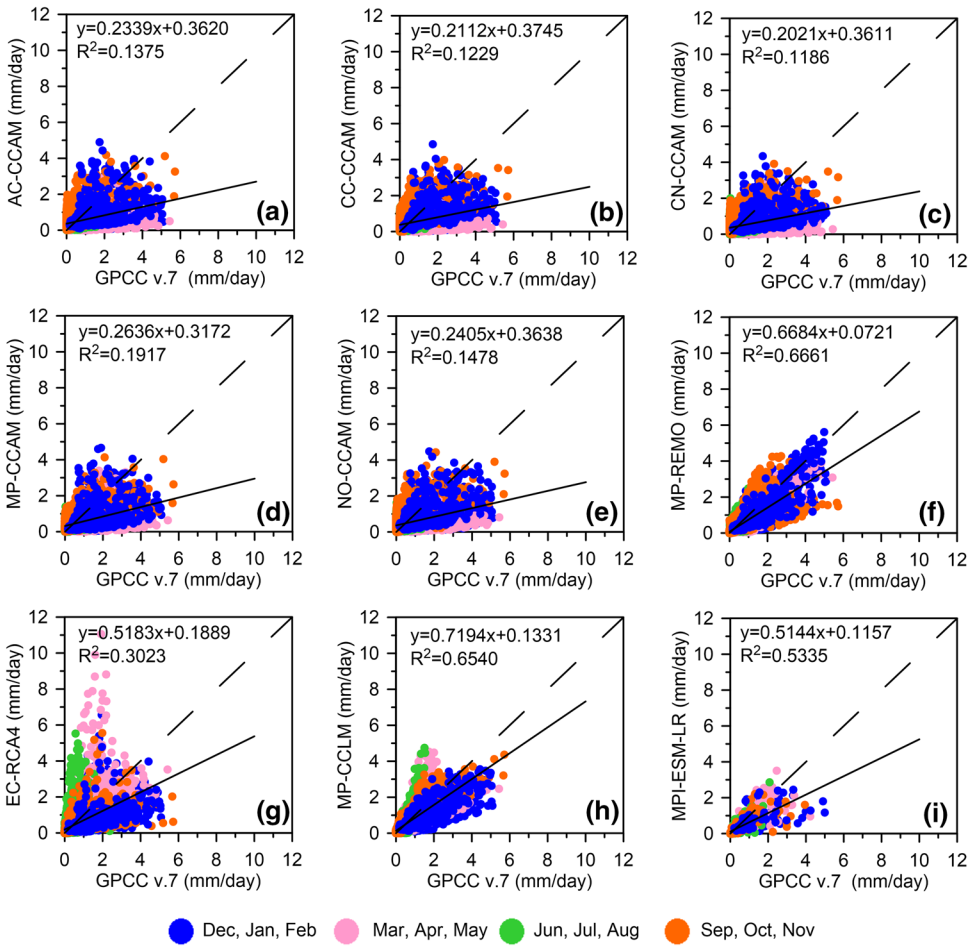

Fig. 6 Comparison of grid points long term average of monthly precipitation (1970–2005) from GPCC v.7 dataset with corresponding values from CORDEX datasets and MPI-ESM-LR GCM

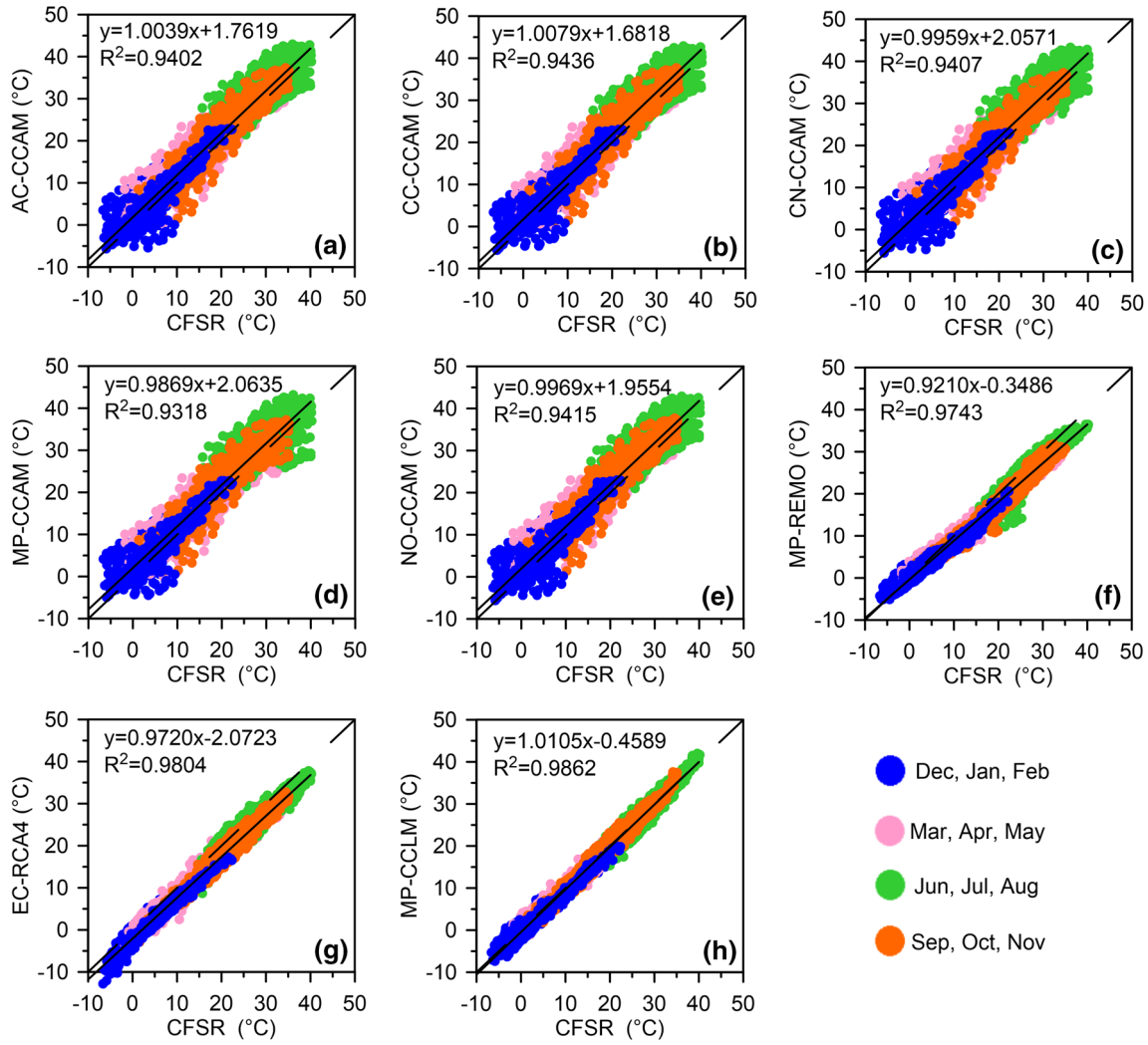

Fig. 7 Comparison of grid points long term average of monthly temperature (1979–2005) from CFSR dataset with corresponding values from CORDEX datasets

Table 8 Correlation coefficient, root mean square error and bias between seasonal precipitation of CORDEX datasets and GPCC v.7 for the period 1970–2005

Dataset	Correlation coefficient				RMSE (mm/day)				Bias (mm/day)			
	DJF	MAM	JJA	SON	DJF	MAM	JJA	SON	DJF	MAM	JJA	SON
AC-CCAM	0.367	0.637	0.010	0.648	1.069	0.797	0.392	0.576	−0.647	−0.650	0.225	0.332
CC-CCAM	0.449	0.657	0.141	0.666	1.036	0.836	0.443	0.560	−0.684	−0.696	0.308	0.320
CN-CCAM	0.410	0.627	0.113	0.706	1.077	0.819	0.440	0.505	−0.726	−0.674	0.292	0.278
MP-CCAM	0.405	0.669	0.022	0.672	1.040	0.764	0.395	0.473	−0.635	−0.624	0.231	0.196
NO-CCAM	0.459	0.650	0.135	0.674	1.044	0.795	0.416	0.568	−0.702	−0.652	0.278	0.336
MP-REMO	**0.836**	**0.916**	0.792	0.725	**0.691**	**0.382**	**0.227**	0.391	−0.497	−0.283	0.118	**0.009**
EC-RCA4	0.636	0.639	0.626	0.638	0.965	0.818	0.551	0.454	−0.704	−0.034	0.204	−0.089
MP-CCLM	0.740	0.849	**0.905**	**0.914**	0.700	0.396	0.230	**0.257**	**−0.402**	**0.005**	**0.021**	0.113
MPI-ESM-LR	0.561	0.774	0.834	0.726	0.883	0.468	0.181	0.474	−0.566	−0.238	−0.035	−0.156

Bold values are the best by season for the CORDEX datasets. In the last row of the Table also performance statistics of MPI-ESM-LR are provided for comparison

Table 9 Correlation coefficient, root mean square error and bias between seasonal temperature of CORDEX datasets and CFSR for the period 1979–2005

Dataset	Correlation coefficient				RMSE (°C)				Bias (°C)			
	DJF	MAM	JJA	SON	DJF	MAM	JJA	SON	DJF	MAM	JJA	SON
AC-CCAM	0.927	0.915	0.844	0.926	2.669	3.024	3.796	2.477	1.569	1.746	2.660	1.356
CC-CCAM	0.927	0.916	0.846	0.926	2.609	2.990	3.706	2.559	1.457	1.712	2.548	1.525
CN-CCAM	0.926	0.916	0.841	0.927	2.832	3.080	3.877	2.534	1.831	1.860	2.755	1.493
MP-CCAM	0.926	0.910	0.786	0.915	2.832	2.939	4.098	2.568	1.831	1.472	2.637	1.437
NO-CCAM	0.927	0.918	0.849	0.927	2.789	3.048	3.673	2.557	1.767	1.835	2.530	1.512
MP-REMO	0.983	0.986	0.951	0.975	1.591	2.085	2.408	2.716	**−0.453**	−1.732	−1.752	−2.468
EC-RCA4	**0.986**	0.984	0.957	0.977	2.522	2.918	2.657	3.087	−2.330	−2.702	−2.210	−2.892
MP-CCLM	0.984	**0.987**	**0.971**	**0.982**	**1.164**	**1.048**	**1.279**	**1.001**	−0.463	**−0.426**	**0.092**	**−0.283**

Bold values are the best by season

observational datasets (even by more than 2 °C in summer) while the others underestimate to different extents.

Overall results achieved for Iran were also evaluated in the six zones identified through the PCA method (Fig. 5), in order to verify if the overall performances of the models were reproduced also locally.

Figure 8, showing the comparison of average monthly percentage precipitation values from CORDEX datasets with GPCC v.7 dataset, highlights that in several cases RCMs are not even able to reproduce the precipitation regime. Specifically, CCAM simulations generally underestimate winter regime and overestimate summer regime in zones 1, 3, 4 and 5, while in zone 2 they anticipate observed regime by about 1 month. In the wettest zone 6, MP-CCLM and EC-RCA4 overestimate spring regime, while CCAM models, though respecting observed regime, systematically underestimate observations. Furthermore, precipitation regime in the dry zone 3 is not reasonably estimated by any RCM. In terms of absolute precipitation values, performance statistics (Table S3 in supplementary material) show that MP-CCLM and MP-REMO are in general the most suitable datasets for all zones, even though in the dry zone 3 also EC-RCA4 provides good results, especially in terms of bias.

As expected, CORDEX datasets match temperature regimes much better than precipitation (Fig. 9). RCMs results for the six zones generally confirm the general behavior, with overestimations from CCAM models (up to almost 3 °C in zone 4) and slighter underestimations from other models. Even though quite high performances are achieved with many RCMs (Table S4 in supplementary material), the

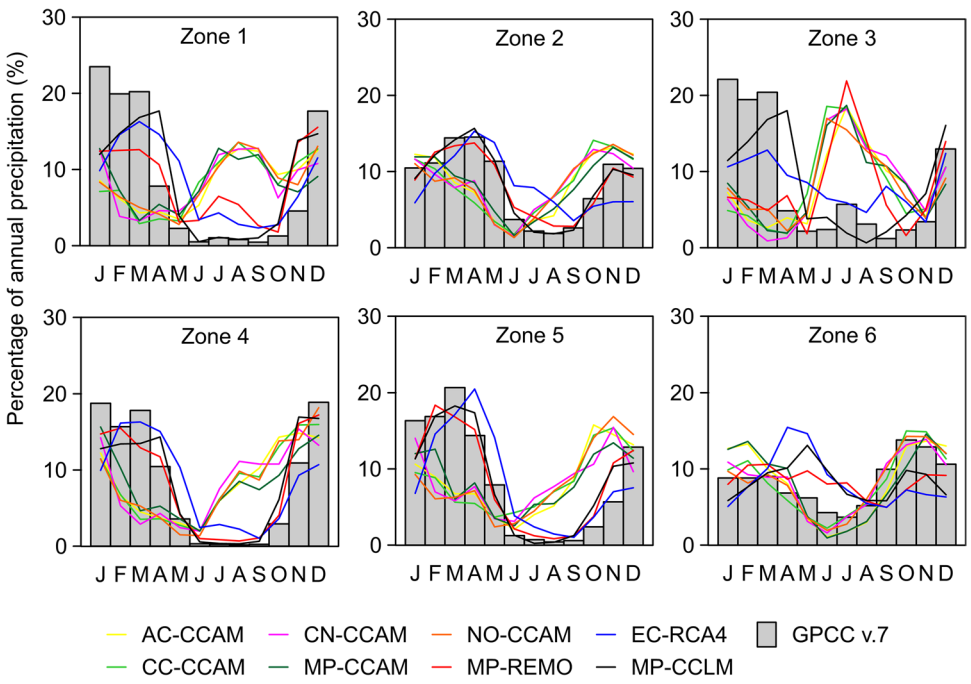

Fig. 8 Comparison of average precipitation regime (as percentage of annual precipitation) from CORDEX datasets with corresponding values from GPCC v.7 dataset for each zone

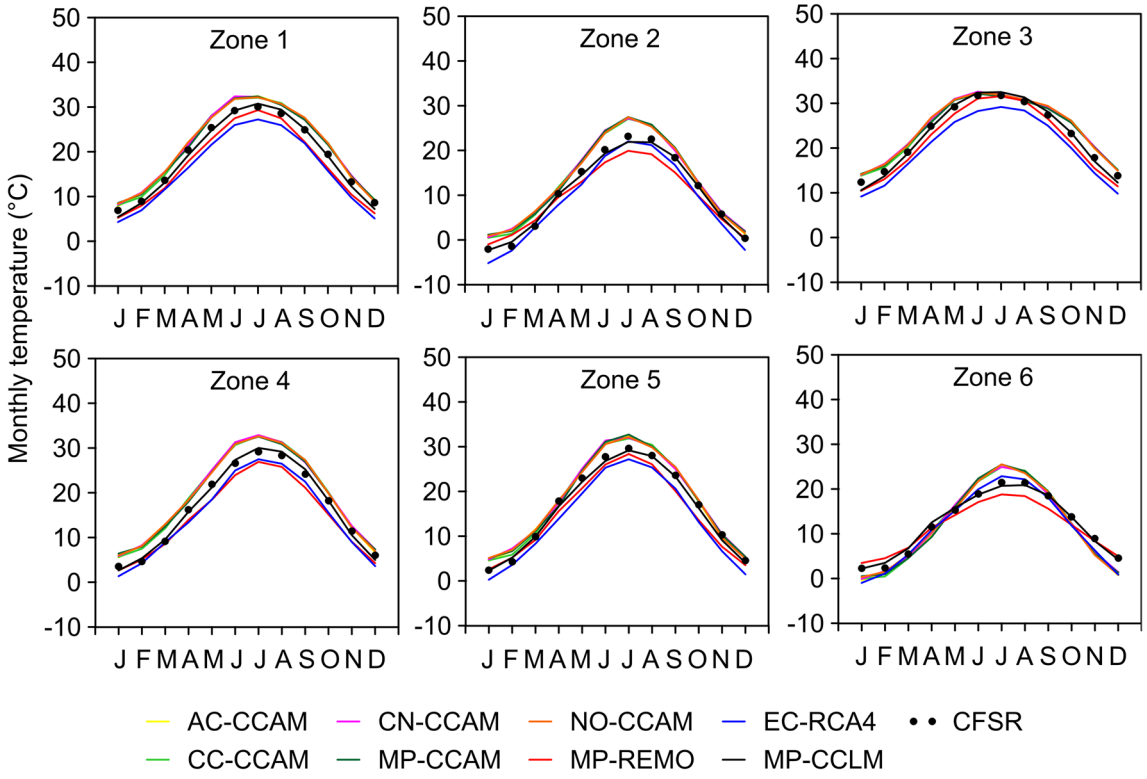

Fig. 9 Comparison of average temperature regime from CORDEX datasets with corresponding values from CFSR dataset for each zone

lowest yearly bias (and in general the best seasonal statistics) is provided by MP-CCLM in all zones.

3.3 RCMs weighting

Comparisons with observational datasets showed that generally MP-CCLM and, secondarily, MP-REMO concerning precipitation, provide the best results. However, statistical indices indicate that their performances are not always dominating and especially for zone 6 other models could add some useful information. For this reason, the model-weighting approach proposed by Coppola et al. (2010) was applied twice. In the first case, all the eight CORDEX South Asia datasets were considered (hereafter Weighted Average 1), in the second case only the three most performing non-CCAM models were used (hereafter Weighted Average 2). In both cases, the first step in the analysis consisted in assessing the reliability of each of the five different weighting methods listed in Table 3, also with respect to a simple unweighted mean. To this aim, both weighted and unweighted seasonal ensembles were compared to the observational gridded datasets. Table 10 shows quite clearly that the first performance indicators combination (i.e. $g_1 \times g_2 \times g_3 \times g_4 \times g_5$, hereafter Case 1) with Weighted Average 2 provides the most accurate statistical indices for seasonal precipitation over Iran. Weighted Average 2—Case 1 maintains in general its good performances also considering the zones individually, except zone 6 (Tables S5 and S6, Supplementary material). In this latter zone, the best performances are generally provided by Weighted Average 1—Case 1, highlighting the usefulness of the CCAM RCMs for a comprehensive analysis of climate change impact in the whole country. Therefore, in the next Sect. 3.4 about climate change projection results, the weighted average considered will be Weighted Average 2—Case 1 but, referring to zone 6, also outcomes provided by Weighted Average 1—Case 1 will be reported.

For the sake of completeness, Table 11 and Tables S7 and S8 (Supplementary Material) show results of the weighting procedure concerning temperature. Indications provided by the statistical indices for this variable are not so clear and univocal as for precipitation but, since the performances of the CORDEX datasets with temperature are generally much higher than with precipitation, information given by the analysis performed over the latter variable was considered prevailing.

Focusing on Table 10, it is noteworthy that, while for both Weighted Average 1 and Weighted Average 2 Case 1–4 do not differ too much each other, they provide always better results than the unweighted case. With Weighted Average 1, the unweighted case is particularly biased by the inaccurate performances of the five CCAM simulations. However, selection of RCMs to include in the weighting procedure is at least as important as the weighting procedure itself:

Table 10 Correlation coefficient, root mean square error and bias between unweighted and weighted seasonal precipitation of CORDEX datasets and GPCC v.7 for the period 1970–2005

Dataset	Correlation coefficient				RMSE (mm/day)				Bias (mm/day)			
	DJF	MAM	JJA	SON	DJF	MAM	JJA	SON	DJF	MAM	JJA	SON
Unweighted Avg. 1	0.633	0.830	0.593	0.776	0.914	0.561	0.292	0.404	−0.625	−0.451	0.210	0.187
Weighted Avg. 1—Case 1	*0.743*	0.889	*0.905*	*0.869*	*0.809*	*0.423*	0.192	*0.304*	*−0.566*	*−0.325*	0.112	*0.112*
Weigh ted Avg. 1—Case 2	0.722	0.884	0.900	0.856	0.832	0.429	0.188	0.320	−0.579	−0.328	0.113	0.121
Weighted Avg. 1—Case 3	0.707	0.879	0.886	0.843	0.848	0.447	0.182	0.333	−0.588	−0.347	0.116	0.130
Weighted Avg. 1—Case 4	0.707	*0.895*	0.818	0.836	0.846	0.465	***0.176***	0.336	−0.587	−0.375	*0.107*	0.124
Weighted Avg. 1—Case 5	0.650	0.788	0.764	0.777	0.903	0.544	0.294	0.401	−0.621	−0.398	0.218	0.181
Unweighted Avg. 2	0.806	0.856	0.861	0.857	0.742	0.397	0.257	0.304	−0.537	−0.104	0.114	***0.011***
Weighted Avg. 2—Case 1	***0.813***	0.908	***0.918***	***0.914***	***0.712***	0.302	0.208	***0.247***	***−0.504***	−0.124	0.082	0.028
Weighted Avg. 2—Case 2	0.812	***0.909***	0.915	0.905	0.715	***0.299***	0.201	0.259	−0.507	−0.125	0.080	0.026
Weighted Avg. 2—Case 3	0.812	0.906	0.913	0.900	0.717	0.305	0.200	0.264	−0.510	−0.121	0.081	0.024
Weighted Avg. 2—Case 4	***0.813***	0.908	0.905	0.901	0.717	0.302	*0.190*	0.262	−0.511	−0.127	***0.076***	0.021
Weighted Avg. 2—Case 5	0.806	0.857	0.862	0.859	0.739	0.394	0.269	0.303	−0.533	***−0.103***	0.118	0.016

Unweighted and Weighted Avg. 1 derive from 8 datasets, Unweighted and Weighted Avg. 2 from the 3 non-CCAM datasets. Italic values are the best by season for each of the two cases, bold values are the absolute best by season

Bold italic values are the absolute best by season

Table 11 Correlation coefficient, root mean square error and bias between unweighted and weighted seasonal temperature of CORDEX datasets and CFSR for the period 1979–2005

Dataset	Correlation coefficient				RMSE (°C)				Bias (°C)			
	DJF	MAM	JJA	SON	DJF	MAM	JJA	SON	DJF	MAM	JJA	SON
Unweighted Avg. 1	0.964	0.961	0.927	0.959	1.660	1.727	2.218	1.471	0.629	0.471	1.158	0.210
Weighted Avg. 1—Case 1	*0.980*	*0.981*	*0.974*	*0.977*	1.251	***1.206***	1.240	1.502	***0.063***	−0.181	−0.451	−1.001
Weighted Avg. 1—Case 2	0.979	*0.981*	*0.974*	0.975	***1.236***	1.211	1.231	1.402	0.226	−0.145	−0.425	−0.823
Weighted Avg. 1—Case 3	0.977	0.978	0.973	0.974	1.310	1.271	***1.213***	***1.342***	0.331	−0.038	−0.265	−0.674
Weighted Avg. 1—Case 4	0.969	0.974	0.968	0.970	1.489	1.382	1.313	1.514	0.324	***−0.032***	***−0.253***	−0.853
Weighted Avg. 1—Case 5	0.974	0.969	0.941	0.964	1.413	1.539	1.906	1.381	0.511	0.347	0.863	***0.198***
Unweighted Avg. 2	***0.991***	***0.991***	***0.979***	0.985	1.495	1.832	1.656	2.077	−1.130	−1.620	−1.290	−1.881
Weighted Avg. 2—Case 1	0.988	0.990	0.978	0.985	1.473	1.665	1.493	2.092	−0.931	−1.394	−1.057	−1.873
Weighted Avg. 2—Case 2	0.989	0.990	0.978	0.985	*1.443*	*1.640*	*1.479*	2.076	*−0.919*	*−1.374*	*−1.041*	−1.867
Weighted Avg. 2—Case 3	0.989	0.990	0.978	0.985	1.446	1.660	1.483	2.067	−0.945	−1.400	−1.047	−1.862
Weighted Avg. 2—Case 4	0.989	0.990	0.977	0.985	1.458	1.687	1.561	2.171	−0.950	−1.425	−1.128	−1.963
Weighted Avg. 2—Case 5	0.991	0.991	0.979	***0.986***	1.470	1.778	1.584	*1.976*	−1.089	−1.565	−1.204	*−1.781*

Bold values are the best by season. Unweighted and Weighted Avg. 1 derive from 8 datasets, Unweighted and Weighted Avg. 2 from the 3 non-CCAM datasets. Italic values are the best by season for each of the two cases, bold values are the absolute best by season

Bold italic values are the absolute best by season

Unweighted Average 2 is always comparable or even better than all combinations of Weighted Average 1.

Figure 10 highlights the level of improvement achieved adopting a weighting approach (Case 1) in precipitation simulations with both Weighted Averages 1 and 2. With Weighted Average 1, especially in zones 1, 4 and 5 winter underestimates and summer overestimates are partially corrected, while the benefit is somehow less marked in the other zones. With Weighted Average 2, the added value of the weighting approach is mostly not evident. Zone 6 is the only where Weighted Average 1 performs better than Weighted Average 2. Differences between different weighted averages or between weighted and unweighted averages are much less evident if temperatures are considered. Weighted (Case 1) and unweighted average curves in Fig. 11 are often overlapping and quite fitting to CFSR dataset. Performance statistics (Table 11 and Tables S7 and S8) show that no particular combination clearly prevails over the others.

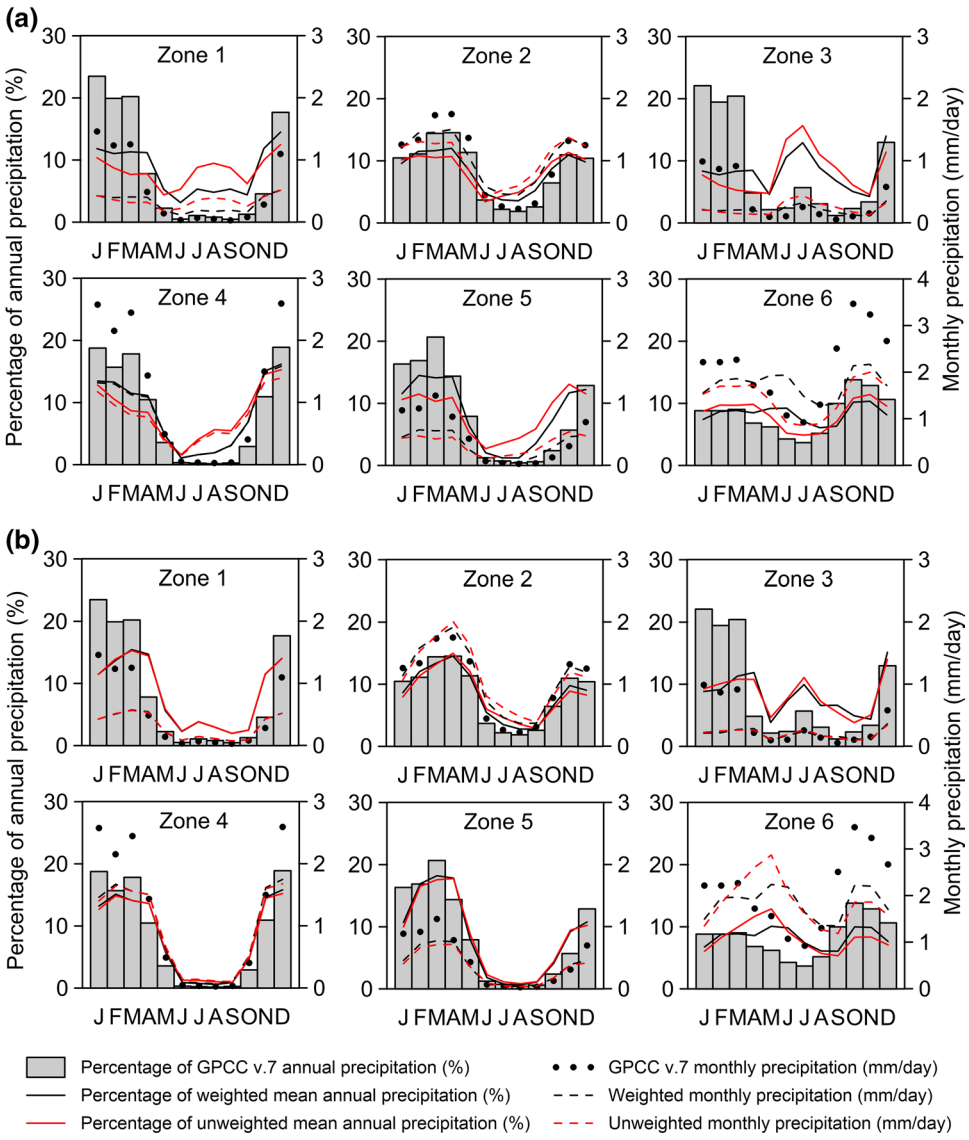

Fig. 10 Comparison of average precipitation regime from both **a** all the eight CORDEX datasets and **b** the three non-CCAM CORDEX datasets weighted (Case 1) and unweighted averages with the corresponding values from GPCC v.7 dataset for each zone

Since Case 1 weighted ensemble was selected for climate change projections (Sect. 3.4), it is interesting to go into details describing single weights of each RCM. Figure 12 provides an overall picture of the influence of each model to the weighted ensemble by season. Significant effects of MP-CCLM and MP-REMO are very clear, while CCAM models and EC-RCA4 weights are closer. Specifically, considering all the eight models (Weighted Average 1) highest impacts (weight greater than 40%) of CCLM are provided on JJA in zones 2, 4, 5 and 6 (highest value of 54%), and on DJF and SON in zone 6. MP-REMO weights more than 40% on DJF and zone 3, on JJA and zone 5 and on MAM and zone 6 (highest value of 53%). CCAM models weights are never greater than 11%. EC-RCA4 shows in general only a slightly better performance, but in the dry zone 3 it provides the highest weights both in JJA and SON, with the highest value of 58%. Considering the weighting procedure with only the three non-CCAM models (Weighted Average 2), highest impacts of CCLM (weight greater than 50%) are found in zones 2 (JJA and SON), 3 (MAM), 4 (JJA), 5 (MAM) and 6 (all seasons but MAM, with the highest value of 68% in winter). MP-REMO weights more than 50% in zones 2 (MAM), 3 (DJF) and 6 (MAM, highest value of 65%), while EC-RCA4 only in zone 3 (SON, highest value of 63%). It should be noted that, even though models impacts are described here in percentage, the sum of the weights is always different if either zonal or seasonal values are added together.

It is noteworthy that the weighted ensemble provides 'reasoned' average results accounting for all available datasets, but it does not ensure necessarily the best statistical performances. Comparing MP-REMO and MP-CCLM performance indices for precipitation (Table 8) with those calculated with Weighted Average 2—Case 1 (Table 10), often the best values are not provided by the ensemble simulation. A similar

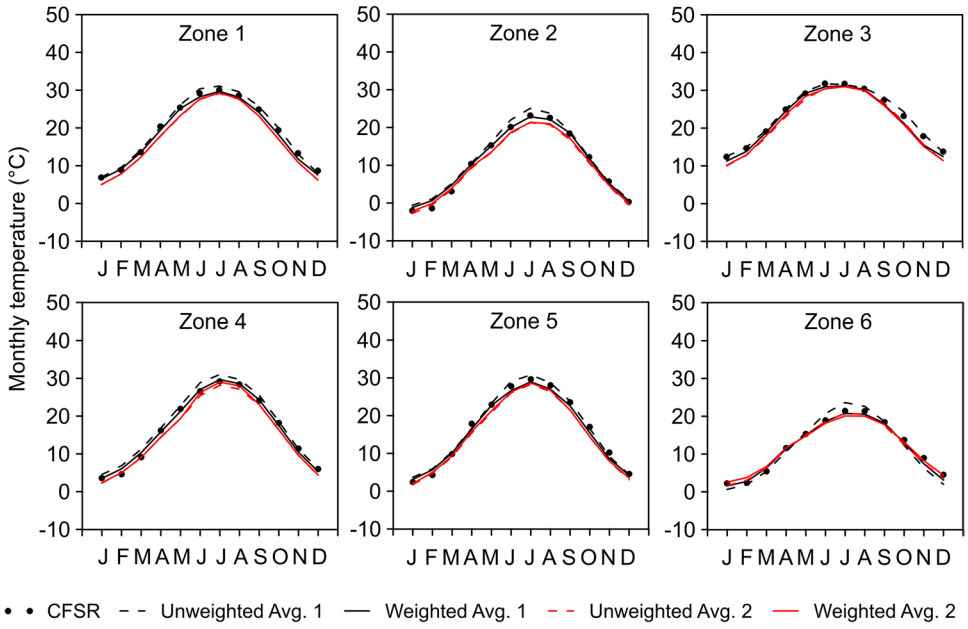

Fig. 11 Comparison of average temperature regime from both all the eight CORDEX datasets (Avg. 1) and the three non-CCAM CORDEX datasets (Avg. 2) weighted (Case 1) and unweighted averages with the corresponding values from CFSR dataset for each zone

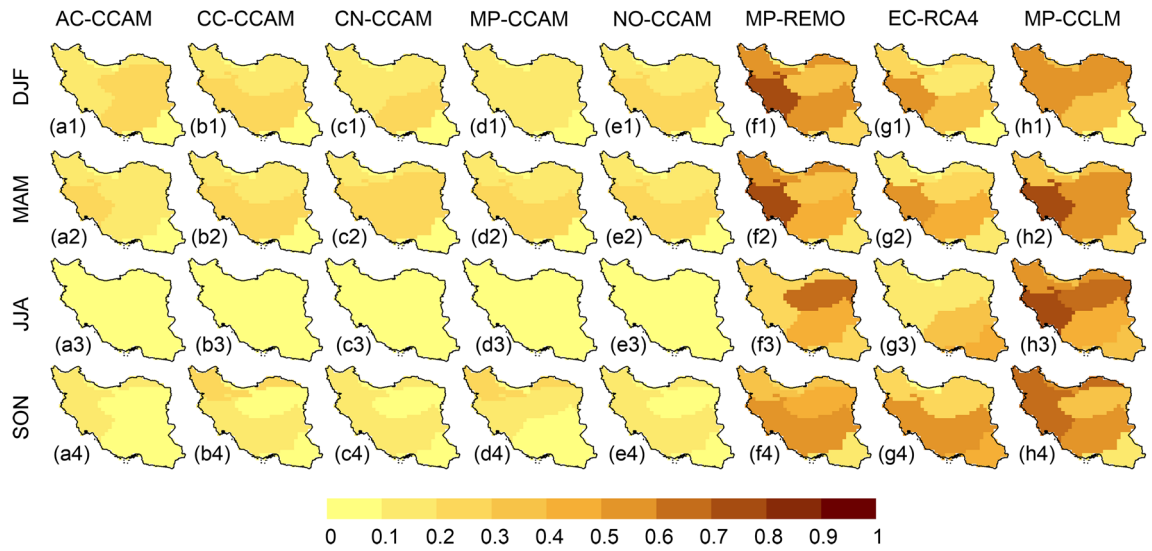

Fig. 12 Weight values for the eight models and all seasons for Case 1

behavior can be observed considering individually the six zones (Tables S3 and S6). The same is also for temperature, considering both the whole Iran (Tables 9, 11) and the individual zones (Tables S4 and S8). Hence, weighted ensemble should be considered as 'a way to reduce the unwanted uncertainty in climate model projections' (Christensen et al. 2010) rather than a reference simulation providing optimal performances. Due to the numerous and varied uncertainty sources, climate prediction must be addressed in a probabilistic sense (e.g., Giorgi 2010), and several efforts are being made for reducing model structural uncertainty through different methods (e.g., Das Bhowmik et al. 2017). Figure 13 provides an overall picture of the weighted approach contribution to the issue of uncertainty reduction in this study showing altogether the seasonal averages of precipitation based on the GPCC v.7 observational dataset, the non-CCAM models unweighted and weighted (Case 1) averages and the MP-CCLM and MP-REMO datasets. Such as highlighted by the performance statistics, unweighted and weighted averages are rather similar and often show an intermediate behavior between MP-CCLM and MP-REMO. Of course, they also include, to different extents, contributions from the third RCM. The weighted average shows improved performances when altogether the 'parent' models have both positive and negative differences

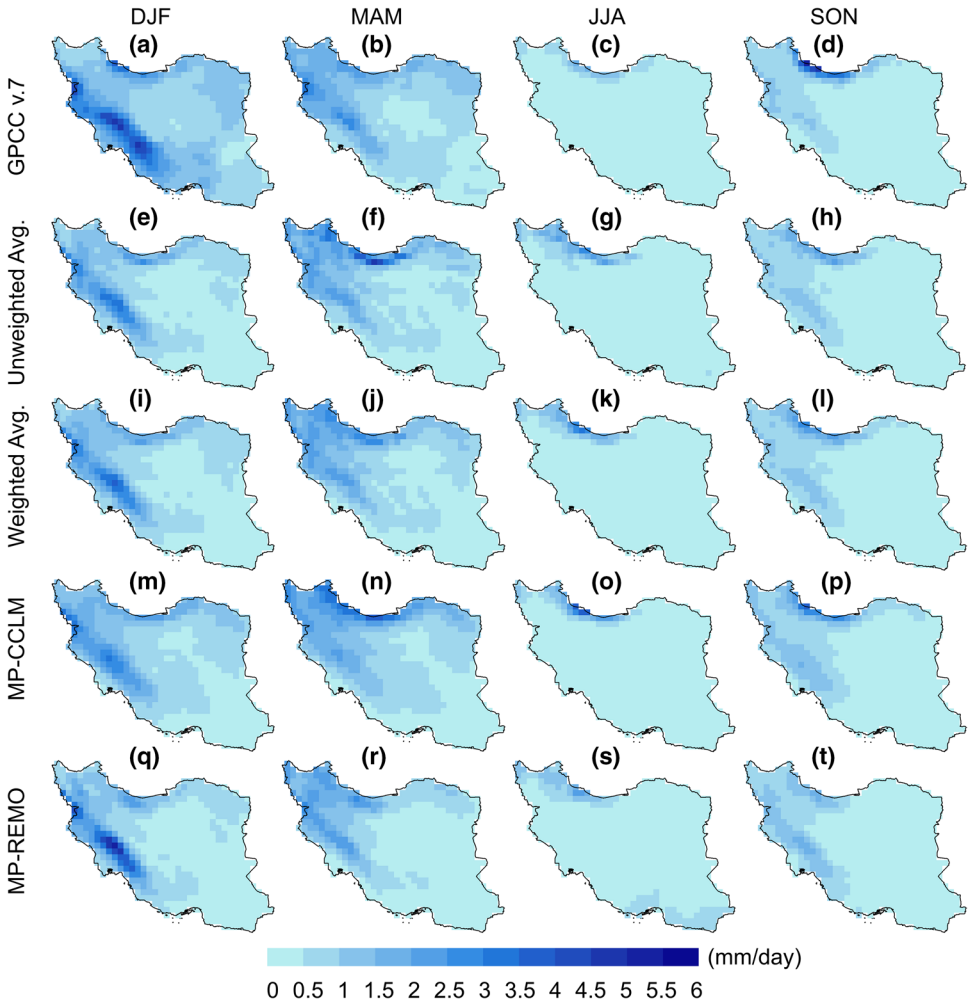

Fig. 13 Long term seasonal average of precipitation based on GPCC v.7, unweighted and weighted average (Case 1) of the three non-CORDEX RCMs, MP-CCLM and MP-REMO for the period 1970–2005

with the observational dataset (e.g. Caspian coast/zone 6 in spring). Instead, if one model already provides very good performances (e.g. MP-REMO along the Zagros Chain/zone 4 in winter), the weighted average biases more or less slightly its results, being affected by the other less performing models. For the sake of completeness, the evaluation of climate change projections in the next Section will show results from all RCMs, focusing especially on MP-REMO and MP-CCLM, together with the weighted and unweighted averages.

3.4 Climate change projections

Hereafter, unless otherwise specified, weighted and unweighted averages refer to Weighted Average 2, involving the three non-CCAM models, and Case 1.

Figures 14 and 15 show respectively the seasonal precipitation and temperature change maps achieved with MP-CCLM, MP-REMO and the weighted and unweighted averages for the future period 2070–2099 with respect to the historical period 1970–2005. Mean annual and seasonal results for the whole Iran and the six zones are summarized in Figs. 16, 17, 18, where also all the other RCMs are shown.

Concerning precipitation, Fig. 14 shows that different increase and decrease patterns can coexist in the same season and model, even though a general reduction trend can be identified. Considering the weighted average, a yearly reduction of − 20.1% in the period 2070–2099 with respect to the period 1970–2005 is projected for the whole country (Fig. 16a), seasonally distributed with − 15.1, − 32.0, − 29.6 and − 5.3%, respectively in winter, spring, summer and autumn (Fig. 17). All zones show a net yearly reduction (from − 11.7% in zone 3 up to − 23.2% in zone 1), even though specific seasonal behaviors were found. Particularly, a strong spring reduction in all areas was achieved, more pronounced along the southern regions (− 42.5, − 49.7 and − 36.7%, respectively in zones 1, 3 and 4), while in autumn positive increases are projected in zones 1, 3 and 5, with higher values in the dry southeastern regions (+ 44.7% in zone 3). For the rainiest zone 6 a yearly reduction of − 20.5% was found (but − 15.8% with Weighted Average 1), and seasonal reductions of − 0.9%

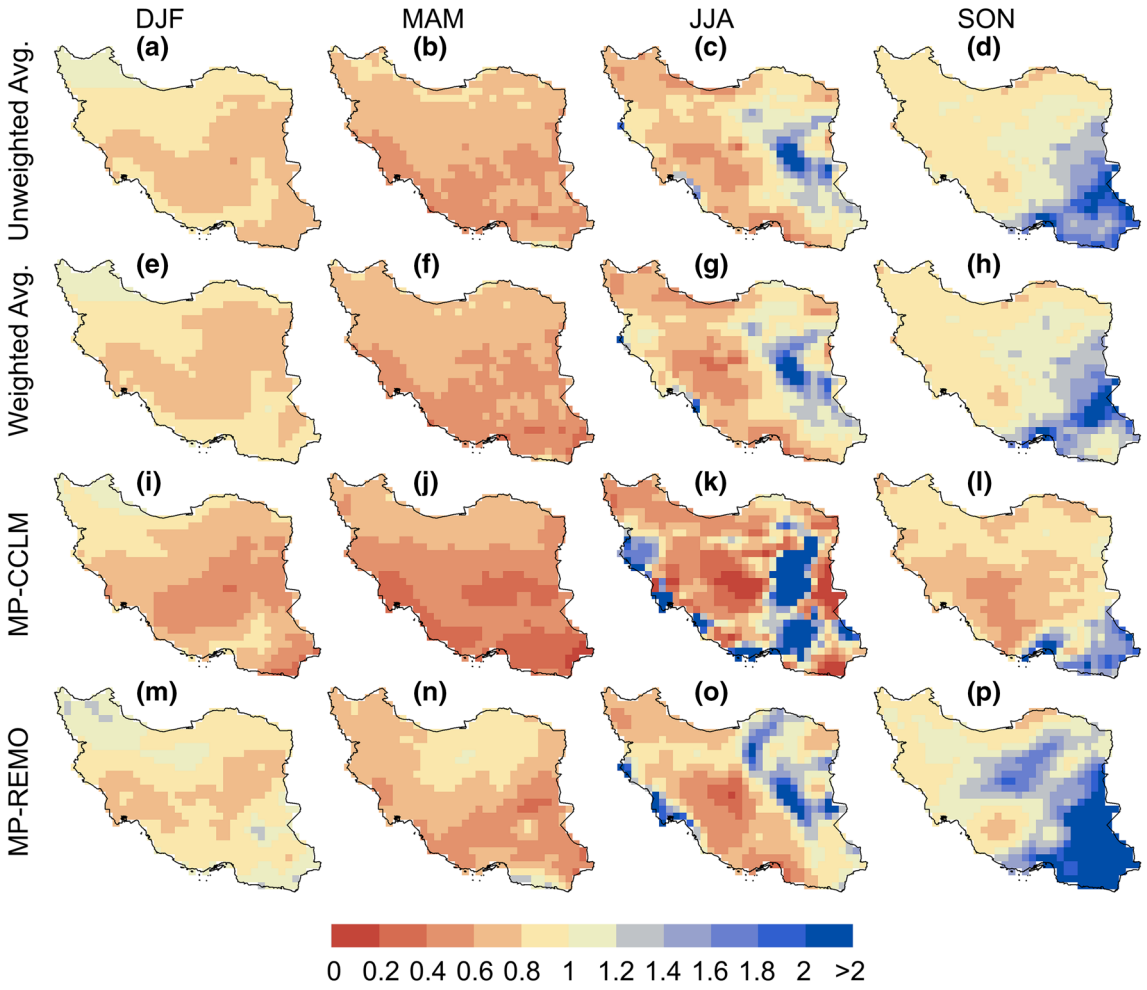

Fig. 14 Maps of the ratio of average seasonal precipitation for future period (2070–2099) vs. historical period (1970–2005) based on MP-CCLM, MP-REMO, weighted and unweighted average of the three non-CCAM RCMs

in DJF, −22.1% in MAM, −44.1% in JJA and −14.8% in SON (+2.6, −21.1, −42.6 and −4.6% with Weighted Average 1, respectively).

With respect to the weighted average, the unweighted average projects a slightly wetter climate, mainly because of the lower impact of MP-CCAM, but overall results are rather similar (maximum difference of 4% in zone 5). The yearly decrease projected by the unweighted average in the country is −18.9%, varying from −29.3% in spring to −3.3% in autumn.

Concerning single models (Figs. 16a, 17), the five CCAM models project mean yearly precipitation increase for both the whole country (ranging from +3.9% with MP-CCAM to +38.1% with AC-CCAM) and the single zones. On the other side, MP-REMO, EC-RCA4 and MP-CCLM all project yearly precipitation reduction both in the whole country (−12.4, −11.2 and −31.0%, respectively) and in the six zones, with the only exception of southeastern zone 3 with MP-REMO (especially due to the autumn increase). MP-CCLM projects by far the driest future climate around the whole country, with the most relevant reductions in zones 1 (−44.4%), 3, 4 and 5, and for all seasons (from −19.7% in autumn to −42.3% in spring, considering the whole country). Such as highlighted with the baseline period, the structural uncertainty determined by the RCM is noteworthy, since MP-CCLM, MP-REMO and MP-CCAM share the same driving GCM and RCP scenario.

The weighted approach certainly does not solve all complex problems related to projections uncertainty. Besides limitations related to the strong background assumptions (e.g., that the ensemble used provides a sufficient description of the uncertainty; Räisänen and Ylhäisi 2012), it has been argued that the weighting itself represents a source of uncertainty (Coppola et al. 2010; Christensen et al. 2010). However, the approach allowed in this case to deal with an ensemble of models providing not univocal climate change projections, accounting for the performances achieved with the baseline period.

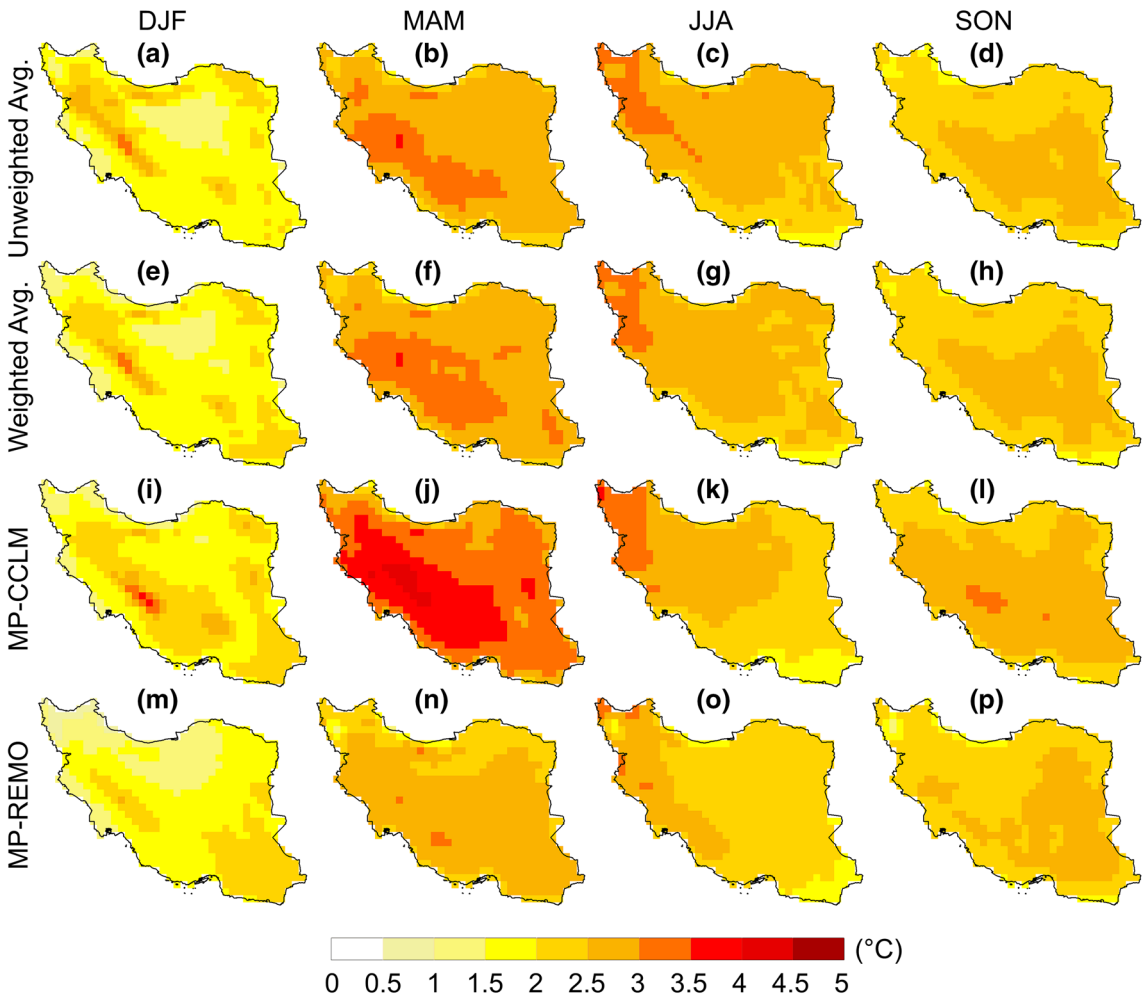

Fig. 15 Maps of the difference of average seasonal temperature for future period (2070–2099) vs. historical period (1979–2005) based on MP-CCLM, MP-REMO, weighted and unweighted average of the three non-CCAM RCMs

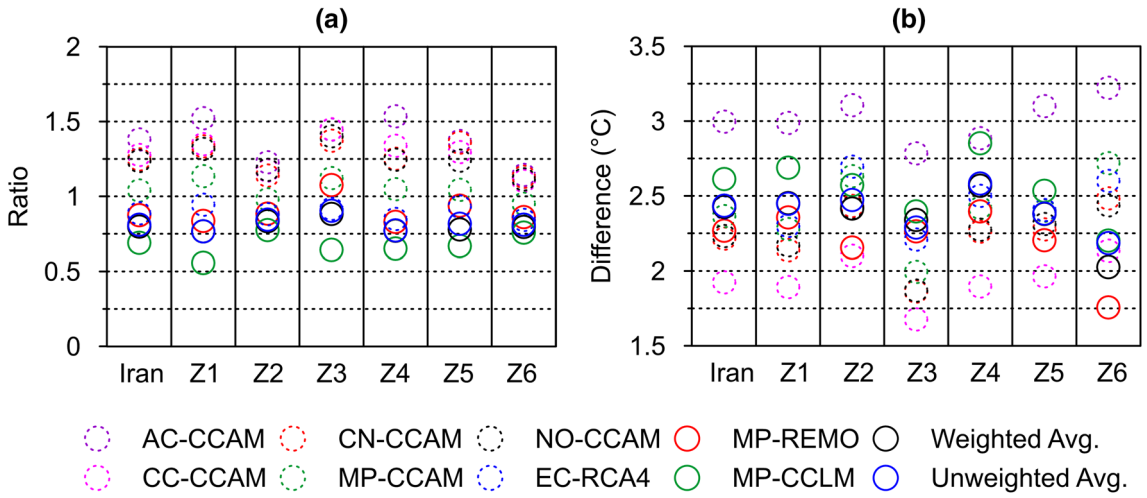

Fig. 16 Ratio (difference) of average annual precipitation (temperature) for future period (2070–2099) vs. historical period (1970–2005) provided by the 8 RCMs and weighted and unweighted averages

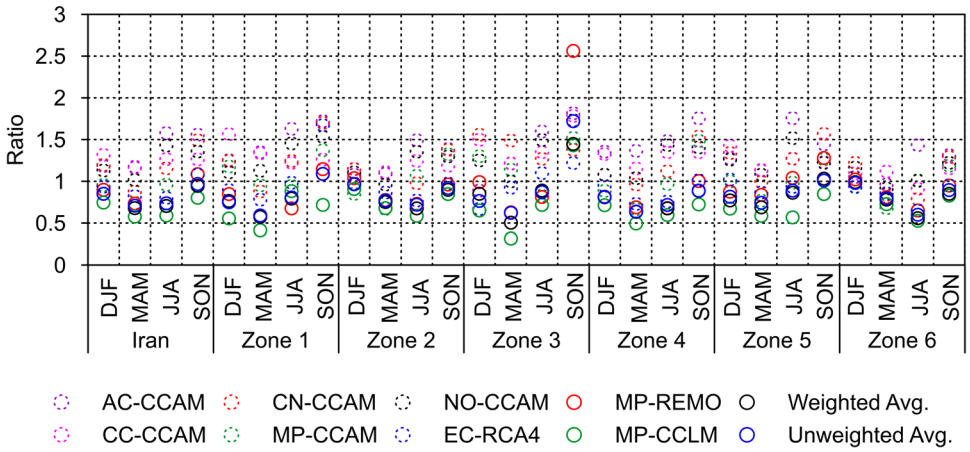

Fig. 17 Ratio of average seasonal precipitation for future period (2070–2099) vs. historical period (1970–2005) provided by the 8 RCMs and weighted and unweighted averages

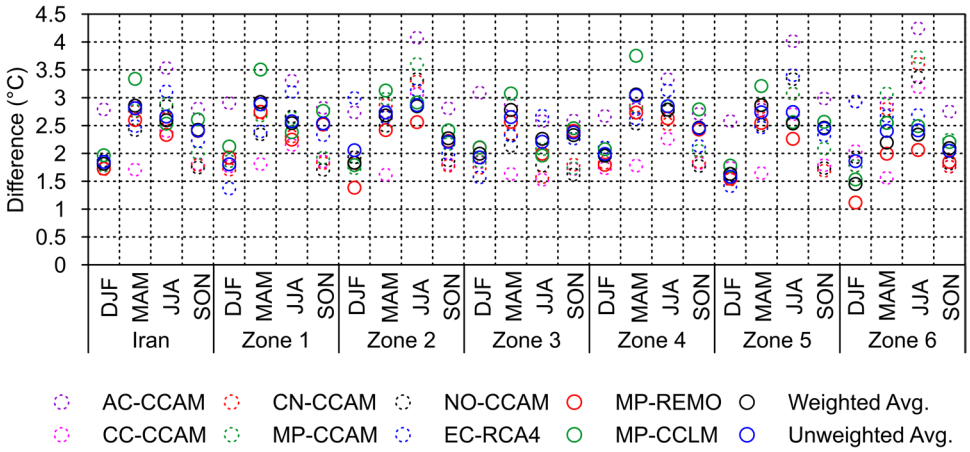

Fig. 18 Difference of average seasonal temperature for future period (2070–2099) vs. historical period (1970–2005) provided by the 8 RCMs and weighted and unweighted averages

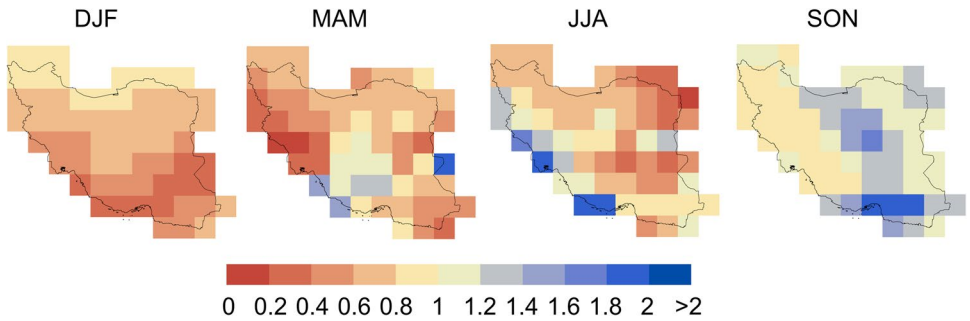

Fig. 19 Maps of the ratio of average seasonal precipitation for future period (2070–2099) vs. historical period (1970–2005) based on MPI-ESM-LR GCM

With respect to previous overall climate change analyses in Iran, precipitation results show some significant differences. In particular, their change pattern is opposite to that showed by Abbaspour et al. (2009), who under different SRES scenarios projected main reductions in the southeastern regions, where we found the lower decrease with the weighted approach. However, results of Abbaspour et al. (2009) derive from older models with a coarser resolution. Global annual maps derived from the CREMA experiment by Coppola et al. (2014) with RegCM under RCP8.5 scenario also showed a non-homogeneous pattern over Iran, but with a slightly prevailing increase (while more marked increase and decrease were showed, respectively, for DJF and JJA). Such as referred in the Introduction, some inconsistencies appear in these results. Finally, the multi-GCM-model analysis performed by Kouhestani et al. (2016) over a large basin in Central Iran confirmed, even though using a lower spatial resolution than that adopted in this study, a general reduction under all RCP scenarios. A comparison carried out in this study between precipitation change projected by both MP-REMO and MP-CCLM (Fig. 14) and their host GCM (Fig. 19) proves a consistent decrease

of rainfall between GCM and RCMs. Yearly precipitation reduction in the whole country projected by MP-ESM-LR is − 18.2%, and also seasonal reductions are in between the two RCMs projections. Nevertheless, the comparison of the results achieved in this study with previous literature suggests that further research is necessary to shed even more light on future precipitation projections uncertainty.

The temperature projections ensemble is more easily interpretable than precipitation, since all models agree in predicting rising temperatures under RCP4.5 scenario, even though with different ranges. Figure 15 shows that in general higher increases are projected for mountain areas and in the warmest seasons. Highest increases up to 4–5 °C are predicted for Zagros chain in spring and northwestern mountainous areas in summer. The weighted average projects a mean annual increase over Iran of + 2.4 °C (Fig. 16b), distributed seasonally with + 1.8, + 2.9, + 2.6 and + 2.4 °C, respectively in winter, spring, summer and autumn (Fig. 18). Similar information is provided by the unweighted average (annual increase of + 2.4 °C, distributed seasonally with + 1.8, + 2.8, + 2.7 and + 2.4 °C). Concerning single RCMs, MP-CCLM provides high temperature increase (+ 2.6 °C annually, distributed seasonally with + 2.0, + 3.3, + 2.5 and + 2.6 °C). The highest annual increase with the weighted average is projected in zone 4 (+ 2.5 °C), where Zagros Mountains are located. Zone 4 is also the zone with the lowest spread between minimum and maximum projected values (1.0 °C, considering also CCAM models), together with zone 2. The weighted average also projects the highest winter (+ 2.0 °C) and spring (+ 3.1 °C) increase in zone 4, while the highest summer increase was found in the northwestern zone 2 (+ 2.8 °C) and the highest autumn increase in zone 1 (+ 2.5 °C). The lowest annual increase (+ 2.1 °C) and almost all the lowest seasonal decreases were found in the wet zone 6 (same results achieved with the Weighted Average 1). Considering all models (including also CCAM models) and seasons (Fig. 18), the absolute maximum increase (+ 4.2 °C) was found with model AC-CCAM and zone 6 in summer, while the minimum increase (+ 1.1 °C) with model MP-REMO and zone 6 in winter.

Summarizing, information provided by all models is rather homogeneous both yearly and seasonally, with differences seldom higher than 1 °C. Temperature increase seems to be influenced by elevation. This issue would deserve a more detailed investigation (such as performed, e.g., by Kotlarski et al. 2012; and; Smiatek et al. 2016), but this analysis goes beyond the objectives of the paper.

The combined effects of temperature increase and precipitation variation on future drought occurrences and intensities was assessed calculating the SC-PDSI time series over each of the 627 0.5°-resolution cells within the Iranian borders. Figure 20 shows the maps of both historical and future periods average SC-PDSI over Iran. Due to the significant projected changes, which turned out to be extremely relevant in some cells, the SC-PDSI range shown in the figure extends far beyond the values traditionally used. Even though all CCAM models project a general increase of precipitation, only three of them (AC-CCAM, CC-CCAM and CN-CCAM) predict a rather widespread increase of the SC-PDSI (about 72% of the cells, with highest values in central and southern areas). NO-CCAM shows an intermediate behavior, with 58.5% cells becoming 'wetter' (mainly in the southeastern zones), while MP-CCAM predicts only 16% of wetter cells, mainly along the southern coast. The latter model (which has the same driving GCM of MP-REMO and MP-CCLM) shares with the non-CCAM models the sharp decrease of SC-PDSI values along the northern regions, particularly over the wet Caspian coasts. EC-RCA4, MP-REMO and MP-CCLM show an overall drying (relative areas of wetter cells equal to 0.5, 3.2 and 0.0%, respectively), with some small increase of SC-PDSI values only with MP-REMO along the southeastern borders. In addition to Caspian coasts, MP-REMO and MP-CCLM show some of the strongest index reductions also in the western and (especially with MP-CCLM) central regions. Also with MP-CCLM, less intense drying in the southern coasts and southeastern borders is projected.

Of course, single models results affect both weighted and unweighted maps, which again show comparable results to each other. Both unweighted and weighted averages project null relative areas with increasing SC-PDSI, and both maintain the sharp SC-PDSI decrease along the Caspian coasts (same results were achieved with Weighted Average 1—Case 1). Furthermore, they show the lowest SC-PDSI values, besides the Caspian coasts, over the western mountainous region (this result is affected by the projected high temperature increase along the Zagros Chain) and in the northeastern region. Again, the region with the lowest SC-PDSI decrease is the southeastern.

The weighted average SC-PDSI maps point out a significant projected reduction of water availability in some of the rainiest zones of Iran. Results highlight the effects of the relative changes in combined precipitation and temperature regimes with respect to a baseline period and provide complementary information to climate change studies based on climatic classification approaches (e.g., Rahimi et al. 2013, which used the De Martonne's classification), where index values are calculated without the need of any reference (i.e. a baseline) period.

Figure 21, showing the frequency distribution of all the monthly SC-PDSI values for all cells in the historical and future periods, highlights that half of the models (namely, all the MPI-ESM-LR-driven and all the non-CCAM) project a negative shift of SC-PDSI values. According to the weighted average map, this shift is stronger in some of the most rainy regions (Caspian coast and Zagros Chain), and weaker in currently dry regions (Southeast of the country). While

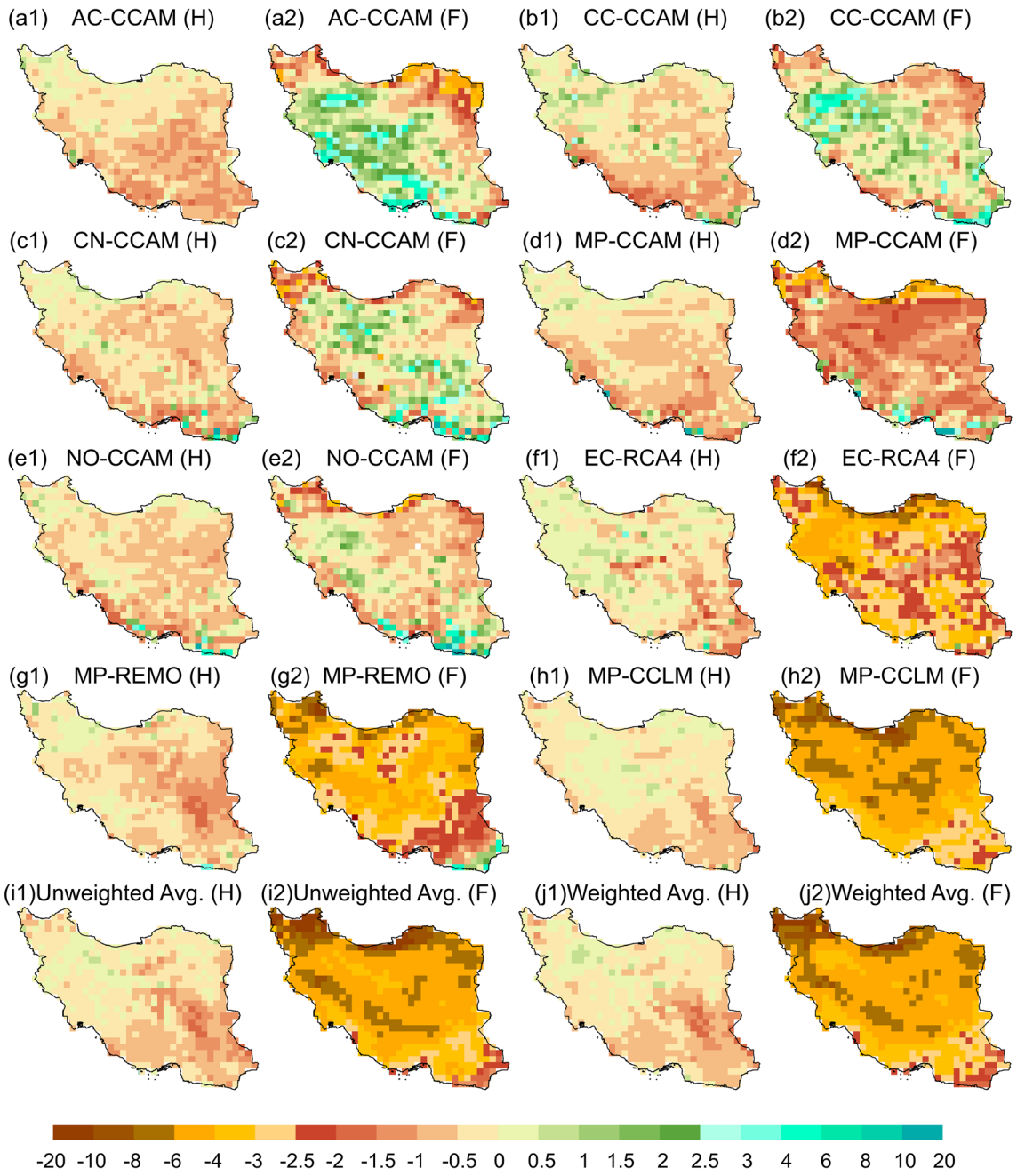

Fig. 20 Maps of the average SC-PDSI for historical (H) and future (F) periods based on the eight RCMs and the weighted and unweighted averages

CCAM models show an increase of the mean of the distribution never higher than 1 point, the other three models show a reduction of more than 3 points (−4.8 with MP-CCLM). In addition, unweighted and weighted average mean reductions were equal to −4.8 and −4.7 points, respectively. Second-moment statistics (namely standard deviation) increased in the future period for all models, generally from 1 to 2 points (but +0.41 for the weighted average) meaning a higher climate variability, with some small wet periods comparable to the historical period, but also with as many extremely dry periods. Water resource management is always more challenging with higher climate variability.

Time and space variabilities of the weighted average over the whole country both in the historical and future periods are summarized in Fig. 22, where time evolution of the mean SC-PDSI value is shown together with the monthly relative area of each PDSI class. The figure clearly highlights the overall climate shift towards a drier scenario. Mean values are almost

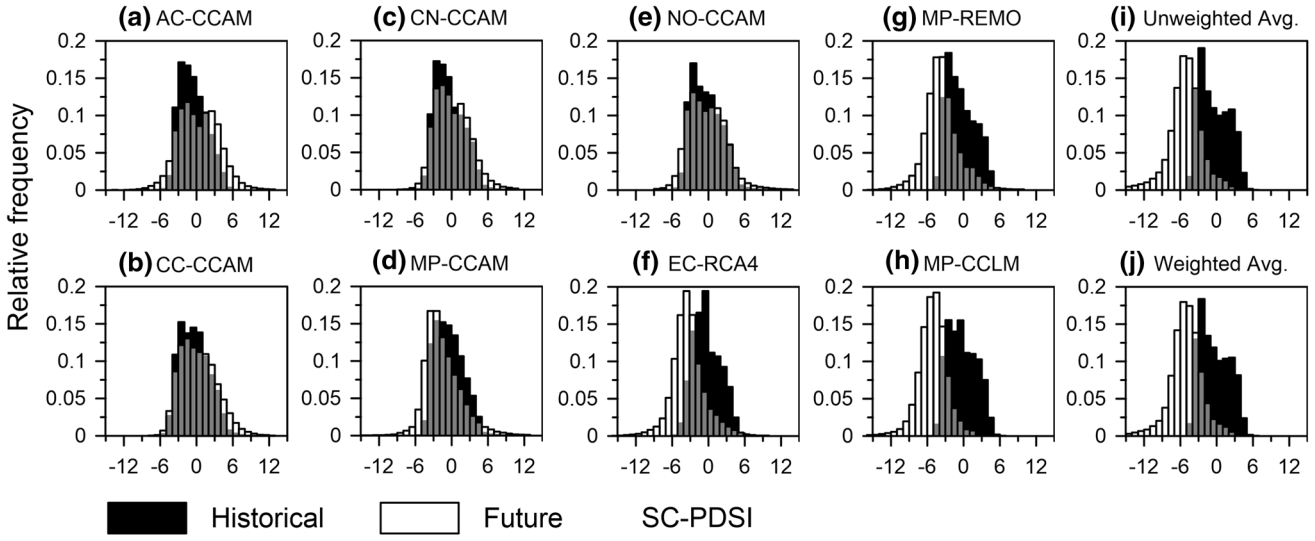

Fig. 21 Histogram of the monthly SC-PDSI for historical and future periods provided by the eight RCMs and the weighted and unweighted averages

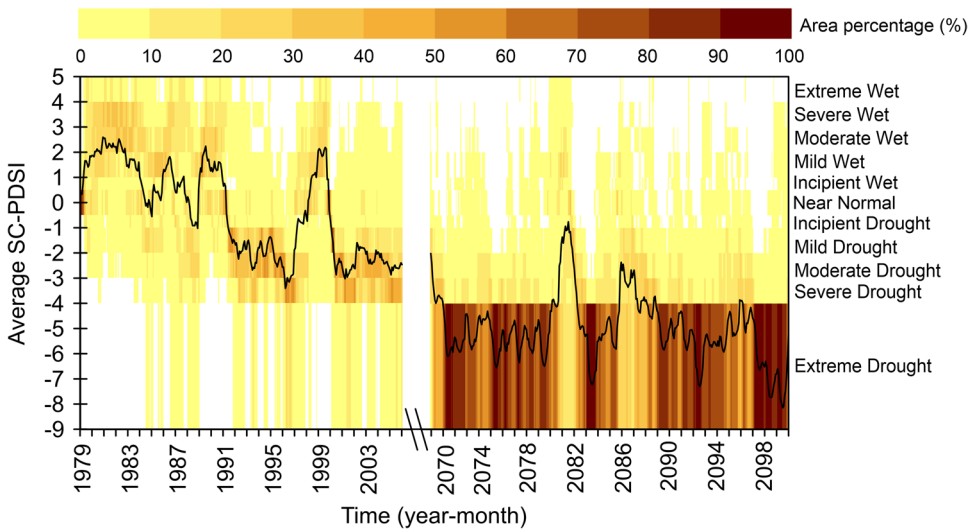

Fig. 22 Time series of the weighted average SC-PDSI over Iran and the monthly relative area of each PDSI class for historical and future periods. The relative areas with null values are indicated by white color

always in the class labeled "extreme drought" according to the baseline period. The relative area falling in this class in the future period is higher than 50% in 81% of the months, and higher than 70% in 53% of the months. If the future scenario projected by the weighted average will come true, drought events currently classified as "extreme" will become "normal", requiring highly effective solutions for water resources management.

4 Conclusions

This paper presented a comprehensive study about projected climate change in Iran at the end of the twenty-first century according to simulations carried out in the framework of the CORDEX South Asia experiment. Preliminary evaluation of RCMs reliability in the baseline period 1970–2005 with eight available models shows that in general MP-CCLM is the most performing concerning both temperature and, together with MP-REMO, precipitation. However, MP-CCLM and MP-REMO performances do not overwhelm the other models for every season and zone in which Iranian territory was divided according to a methodology based on PCA, hence a weighting approach was adopted in order to take into account useful information from each of the models. Some experiments were carried out using either all the eight available models or only the generally most performing three non-CCAM models. These experiments showed that the selection of the RCMs

to include in the weighting procedure can be even more important than the weighting itself.

Weighted precipitation projections for the future period show an overall decrease of 20% and particularly marked reductions in spring and summer. This reduction is consistent with the outcomes of MPI-ESM-LR, which is the host GCM of the most performing RCMs analyzed. Temperature projections provide an overall mean annual increase of 2.4 °C, predicted by both weighted and unweighted averages.

Weighted future drought scenarios, depicted by means of the SC-PDSI index accounting for both temperature and precipitation variations, predict a sharp drying that can be configured as a real shift in mean climate conditions, affecting drastically the water resources of the country, especially in the wetter areas like the Caspian coast.

Though considering a relatively high number of new high-resolution climate change datasets, this study unavoidably suffers from several and 'typical' weaknesses related at least to: (1) the assumption that the model ensemble considered explains sufficiently the future uncertainty; (2) actual reliability and limits of the weighting method, that were partially investigated in this paper; (3) scenario uncertainty; (4) structural uncertainty of both GCMs and RCMs (from this point of view, the differences between MPI-ESM-LR-driven RCMs provide useful insights); (5) simplified impact on water resources availability determined by a 'simple' drought index; (6) spatial resolution of climate models and, to a lesser extent, spatial resolution and reliability of observational analysis/reanalysis datasets.

Some of the drawbacks listed are being resolved. For example, a big effort is going on for increasing resolution of global hydrological modelling (Bierkens et al. 2015; Singh et al. 2015), for a more detailed description of the impact on water resources through interaction with hydrological models (e.g., Senatore et al. 2011; Ravazzani et al. 2015), for a better description of surface hydrology-atmosphere interactions in climate models (e.g., Gochis et al. 2013; Senatore et al. 2015). Some other problems can be addressed by increasing the number of GCMs and RCMs involved in the analysis, while some others still need much investigation. However, the permanent shift in climate conditions in Iran achieved with the most reliable models in this study, with much more drought periods that today would be classified as extreme, clearly suggests to be prepared and work to improve deeply current water resources management.

Acknowledgements The authors thank the Executive Editor Susanna Corti and the anonymous reviewers for their critical and constructive reviews, which helped to improve the quality of the paper. They acknowledge the World Climate Research Programme's Working Group on Regional Climate, and the Working Group on Coupled Modelling, former coordinating body of CORDEX and responsible panel for CMIP5. They also thank the climate modelling groups (listed in Table 2 of this paper) for producing and making available their model outputs and acknowledge the Earth System Grid Federation infrastructure, an international effort led by the U.S. Department of Energy's Program for Climate Model Diagnosis and Intercomparison, the European Network for Earth System Modelling and other partners in the Global Organisation for Earth System Science Portals (GO-ESSP). The GPCC v.7 dataset is provided by NOAA/OAR/ESRL/PSD, Boulder, Colorado, USA, the CRU-TS v.3.23 dataset by the Climatic Research Unit, University of East Anglia, the CFSR dataset by the Climate Forecast System Reanalysis (CFSR) project carried out by the Environmental Modelling Center (EMC), National Centers for Environmental Prediction (NCEP). The European Centre for Medium-Range Weather Forecasts (ECMWF) provides the access to the ERA-Interim and ERA-20C datasets. The Iranian Meteorological Organization (IRIMO) is appreciated for providing the observed data. The Oak Ridge National Laboratory Distributed Active Archive Center (ORNL DACC) is appreciated for providing the soil water-holding capacity dataset. Somayeh Hejabi gratefully acknowledges Iranian Ministry of Science, Research and Technology (MSRT) for the financial support during her stay in Italy in the period January-August 2016.

References

Abbaspour KC, Faramarzi M, Ghasemi SS, Yang H (2009) Assessing the impact of climate change on water resources in Iran. Water Resour Res 45:W10434

Almazroui M (2016) RegCM4 in climate simulation over CORDEX-MENA/arab domain: selection of suitable domain, convection and land-surface schemes. Int J Climatol 36(1):236–251

Almazroui M, Islam M, Al-Khalaf AK, Saeed F (2016) Best convective parameterization scheme within RegCM4 to downscale CMIP5 multi-model data for the CORDEX-MENA/arab domain. Theor Appl Climatol 124(3):807–823

Azari M, Moradi HR, Saghafian B, Faramarzi M (2016) Climate change impacts on streamflow and sediment yield in the North of Iran. Hydrol Sci J 61(1):123–133

Bierkens MFP, Bell VA, Burek P, Chaney N, Condon L, David CH, de Roo A, Döll P, Drost N, Famiglietti JS, Flörke M, Gochis DJ, Houser P, Hut R, Keune J, Kollet S, Maxwell R, Reager JT, Samaniego L, Sudicky E, Sutanudjaja EH, van de Giesen N, Winsemius H, Wood EF (2015) Hyper-resolution global hydro-logical modelling: what is next? Hydrol Process 29:310–320

Boé J, Terray L (2015) Can metric-based approaches really improve multi-model climate projections? The case of summer temperature change in France. Clim Dyn 45:1913–1928

Bucchignani E, Mercogliano P, Rianna G, Panitz H-J (2016a) Analysis of ERA-Interim-driven COSMO-CLM simulations over Middle East–North Africa domain at different spatial resolutions. Int J Climatol 36:3346–3369

Bucchignani E, Cattaneo L, Panitz HJ, Mercogliano P (2016b) Sensitivity analysis with the regional climate model COSMO-CLM over the CORDEX-MENA domain. Meteorol Atmos Phys 128:73–95

Cattel RB (1966) The scree test for the number of factors. Multivar Behav Res 1:245–276

Christensen JH, Kjellström EK, Giorgi F, Lenderink G, Rummukainen M (2010) Weight assignment in regional climate models. Clim Res 44:179–194

Coppola E, Giorgi F, Rauscher SA, Piani C (2010) Model weighting based on mesoscale structures in precipitation and temperature in an ensemble of regional climate models. Clim Res 44:121–134

Coppola E, Giorgi F, Raffaele F, Fuentes-Franco R, Giuliani G, Llopart-Pereira M, Mamgain A, Mariotti L, Diro GT, Torma C (2014)

Present and future climatologies in the phase I CREMA experiment. Clim Change 125:23–38
Das Bhowmik R, Sharma A, Sankarasubramanian A (2017) Reducing Model structural uncertainty in climate model projections—a rank-based model combination approach. J Clim 30(24):10139–10154
Dash SK, Mishra SK, Pattnayak KC, Manmgain A, Mariotti L, Coppola E, Giorgi F, Giuliani G (2015) Projected seasonal mean summer monsoon over India and adjoining regions for the twenty-first century. Theor Appl Climatol 122:581–593
Dee DP et al (2011) The ERA-Interim reanalysis: configuration and performance of the data assimilation system. Q J R Meteorol Soc 137:553–597. https://doi.org/10.1002/qj.828
Dinpashoh Y, Fakheri-Fard A, Moghaddam M, Jahanbakhsh S, Mirnia M (2004) Selection of variables for the purpose of regionalization of Iran's precipitation climate using multivariate methods. J Hydrol 297:109–123. https://doi.org/10.1016/j.jhydrol.2004.04.009
Dobler A, Ahrens B (2008) Precipitation by a regional climate model and bias correction in Europe and South Asia. Meteorol Z 17:499–509
Domroes M, Kaviani M, Schaefer D (1998) An analysis of regional and intraannual precipitation variability over Iran using multivariate statistical methods. Theor Appl Climatol 61:151–159. https://doi.org/10.1007/s007040050060
Emam AR, Kappas M, Hosseini SZ (2015) Assessing the impact of climate change on water resources, crop production and land degradation in a semi-arid river basin. Hydrol Res 46(6):854–870
Etemadi H, Samadi SZ, Sharifikia M, Smoak JM (2016) Assessment of climate change downscaling and non-stationarity on the spatial pattern of a mangrove ecosystem in an arid coastal region of southern Iran. Theor Appl Climatol 126:35–49
Fatichi S, Ivanov VY, Paschalis A, Peleg N, Molnar P, Rimkus S, Kim J, Burlando P, Caporali E (2016) Uncertainty partition challenges the predictability of vital details of climate change. Earth's Future 4:240–251
Ghimire S, Choudary A, Dimri AP. (2015) Assessment of the performance of CORDEX-South Asia experiments for monsoonal precipitation over the Himalayan region during present climate: part I. Clim Dyn. https://doi.org/10.1007/s00382-015-2747-2
Giorgi F (2010) Uncertainties in climate change projections, from the global to the regional scale. EPJ Web Conf 9:115–129, https://doi.org/10.1051/epjconf/201009009
Giorgi F (2014) Introduction to the special issue: the phase I CORDEX RegCM4 hyper-matrix (CREMA) experiment. Clim Change 125:1–5
Giorgi F, Gutowsky WJ (2016) Coordinated experiments for projections of regional climate change. Curr Clim Change Rep 2:202–210
Giorgi F, Mearns LO (2002) Calculation of average, uncertainty range and reliability of regional climate changes from AOGCM simulations via the 'reliability ensemble averaging (REA)' method. J Clim 15:1141–1158
Giorgi F, Jones C, Asrar G (2009) Addressing climate information needs at the regional scale: the CORDEX framework. WMO Bull 58:175–183
Giorgi F, Coppola E, Solmon F et al (2012) RegCM4: model description and preliminary tests over multiple CORDEX domains. Clim Res 52:7–29
Giorgi F, Coppola E, Raffaele F et al (2014) Change in extremes and hydroclimatic regimes in the CREMA ensemble projections. Clim Chang 125:39–51
Gochis DJ, Yu W, Yates DN (2013) The WRF-Hydro model technical description and user's guide, version 1.0. NCAR technical document. https://ral.ucar.edu/projects/wrf_hydro/overview. Accessed 28 Feb 2018
Harris I, Jones P, Osborn T, Lister D (2014) Updated high-resolution grids of monthly climatic observations–the CRU TS3. 10 Dataset. Int J Climatol 34:623–642. https://doi.org/10.1002/joc.3711
Hashemi H, Uvo CB, Berndtsson R (2015) Coupled modeling approach to assess climate change impacts on groundwater recharge and adaptation in arid areas. Hydrol Earth Syst Sci 19:4165–4181
Hingray B, Saïd M (2014) Partitioning internal variability and model uncertainty components in a multimember multimodel ensemble of climate projections. J Clim 27:6779–6798
IPCC (2007) Climate change 2007: impacts, adaptation, and vulnerability. In: Parry ML et al (eds) Contribution of working group II to the third assessment report of the intergovernmental panel on climate change. Cambridge Univ. Press, Cambridge
Juneng L, Tangang F, Chung JX, Ngai ST, The TW, Narisma G, Cruz F, Phan-Van T, Ngo-Duc T, Santisirisomboon J, Singhruck P, Gunawan D, Aldrian E (2016) Sensitivity of the Southeast Asia rainfall simulations to cumulus and ocean flux parameterization in RegCM4. Clim Res 69:59–77. https://doi.org/10.3354/cr01386
Kotlarski S, Bosshard T, Lüthi D, Pall P, Schär C (2012) Elevation gradients of European climate change in the regional climate model COSMO-CLM. Clim Change 112:189–215
Kotlarski S, Keuler K, Christensen OB, Colette A, Déqué M, Gobiet A, Görgen K, Jacob D, Lüthi D, van Meijgaard E, Nikulin G, Schär C, Teichmann C, Vautard R, Warrach-Sagi K, Wulfmeyer V (2014) Regional climate modeling on European scales: a joint standard evaluation of the EURO-CORDEX RCM ensemble. Geosci Model Dev 7(1):217–293
Kouhestani S, Eslamian SS, Abedi-Koupai J, Besalatpour AA (2016) Projection of climate change impacts on precipitation using soft-computing techniques: a case study in Zayandeh-rud Basin, Iran. Glob Planet Change 144:158–170
Lawley DN (1956) Tests for significance for the latent roots of covariance and correlation matrices. Biometrica 43:128–136
Li H, Xu CY, Beldring S et al (2016) Water Resources under climate change in Himalayan Basins. Water Resour Manag 30(2):843–859
McGregor JL, Dix MR (2001) The CSIRO conformal-cubic atmospheric GCM. In: Hodnett PF (ed) IUTAM symposium on advances in mathematical modelling of atmosphere and ocean dynamics. Kluwer, Dordrecht, pp 197–202
Meehl G, Covey C, Delworth T, Latif M, McAvaney B, Mitchell JFB, Stouffer RJ, Taylor KE (2007) The WCRP CMIP3 multimodel dataset. A new era in climate change research. Bull Am Meteorol Soc 88(2007):1383–1394
Modarres R, Sarhadi A (2011) Statistically-based regionalization of rainfall climates of Iran. Glob Planet Change 75:67–75. https://doi.org/10.1016/j.gloplacha.2010.10.009
Moss RH et al (2010) The next generation of scenarios for climate change research and assessment. Nature 463:747–756
Naderi M, Raeisi E (2016) Climate change in a region with altitude differences and with precipitation from various sources, South-Central Iran. Theor Appl Climatol 124:529–540
Ngo-Duc T, Tangang FT, Santisirisomboon J, Cruz F, Trinh-Tuan L, Nguyen-Xuan T, Phan-Van T, Juneng L, Narisma G, Singhruck P, Gunawan D, Aldrian E (2017) Performance evaluation of RegCM4 in simulating extreme rainfall and temperature indices over the CORDEX-Southeast Asia Region. Int J Climatol 37:1634–1647. https://doi.org/10.1002/joc.4803
North GR, Bell TL, Calahan RF (1982) Sampling errors in the estimation of empirical orthogonal functions. Mon Weather Rev 110:699–706
Palmer WC (1965) Meteorological drought, vol 30. US Department of Commerce, Weather Bureau Washington, DC
Pechlivanidis IG, Olsson J, Bosshard T, Sharma D, Sharma KC (2016) Multi-basin modelling of future hydrological fluxes in the indian subcontinent. Water 8(5):177. https://doi.org/10.3390/w8050177

Poli et al (2016) ERA-20C: An atmospheric reanalysis of the twentieth century. J Clim. https://doi.org/10.1175/JCLI-D-15-0556.1

Prein A, Gobiet A, Truhetz H, Keuler K, Goergen K, Teichmann C et al (2016) Precipitation in the EURO-CORDEX 0.11° and 0.44° simulations: high resolution, high benefits? Clim Dyn 46:383–412

Rahimi J, Ebrahimpour M, Khalili A (2013) Spatial changes of extended De Martonne climatic zones affected by climate change in Iran. Theor Appl Climatol 112:409–418

Rahmani MA, Zarghami M (2013) A new approach to combine climate change projections by ordered weighting averaging operator; applications to northwestern provinces of Iran. Glob Planet Change 102:41–50

Räisänen J, Ylhäisi J (2012) Can model weighting improve probabilistic projections of climate change? Clim Dyn 39:1981–1998

Räisänen J, Ruokolainen L, Ylhäisi J (2010) Weighting of model results for improving best estimates of climate change. Clim Dyn 35:407–422

Raju PSV, Bhatla R, Almazroui M, Assiri A (2015) Performance of convection schemes on the simulation of summer monsoon features over the South Asia CORDEX domain using RegCM-4.3. Int J Climatol 35:4695–4706

Ravazzani G, Barbero S, Salandin A, Senatore A, Mancini M (2015) An integrated hydrological model for assessing climate change impacts on water resources of the Upper Po river basin. Water Resour Manag 29(4):1193–1215

Raziei T (2017) A precipitation regionalization and regime for Iran based on multivariate analysis. Theor Appl Climatol. https://doi.org/10.1007/s00704-017-2065-1

Raziei T, Bordi I, Pereira LS (2011) An application of GPCC and NCEP/NCAR datasets for drought variability analysis in Iran. Water Resour Manag 25:1075–1086. https://doi.org/10.1007/s11269-010-9657-1

Raziei T, Mofidi A, Santos JA, Bordi I (2012) Spatial patterns and regimes of daily precipitation in Iran in relation to large-scale atmospheric circulation. Int J Climatol 32:1226–1237

Rechid D, Raddatz TJ, Jacob D (2009) Parameterization of snow-free land surface albedo as a function of vegetation phenology based on MODIS data and applied in climate modelling. Theor Appl Climatol 95:245

Rencher AC (1998) Multivariate statistical inference and applications. Wiley-Interscience, New York

Saha S et al (2010) The NCEP climate forecast system reanalysis. Bull Am Meteorol Soc 91:1015

Samuelsson P et al (2011) The Rossby centre regional climate model RCA3: model description and performance. Tellus 63A:4–23

Sarmadi F, Shokoohi A (2015) Regionalizing precipitation in Iran using GPCC gridded data via multivariate analysis and L-moment methods. Theor Appl Climatol 122:121–128. https://doi.org/10.1007/s00704-014-1292-y

Sayari N, Bannayan M, Alizadeh A, Farid A (2013) Using drought indices to assess climate change impacts on drought conditions in the northeast of Iran (case study: Kashafrood basin). Meteorol Appl 20:115–127

Schneider U, Becker A, Finger P, Meyer-Christoffer A, Rudolf B, Ziese M (2015) GPCC full data reanalysis version 7.0 at 0.5°: monthly land-surface precipitation from rain-gauges built on GTS-based and historic data. https://doi.org/10.5676/DWD_GPCC/FD_M_V.7_050

Senatore A, Mendicino G, Smiatek G, Kunstmann H (2011) Regional climate change projections and hydrological impact analysis for a Mediterranean basin in southern Italy. J Hydrol 399(1–2):70–92

Senatore A, Mendicino G, Gochis DJ, Yu W, Yates DN, Kunstmann H (2015) Fully coupled atmosphere-hydrology simulations for the Central Mediterranean: impact of enhanced hydrological parameterization for short- and long-timescales. J Adv Model Earth Syst 7(4):1693–1715

Singh RS, Reager JT, Miller NL, Famiglietti JS (2015) Toward hyper-resolution land-surface modeling: the effects of fine-scale topography and soil texture on CLM4.0 simulations over the Southwestern U.S. Water Resour Res 51:2648–2667. https://doi.org/10.1002/2014WR015686

Smiatek G, Kunstmann H, Senatore A (2016) EURO-CORDEX regional climate model analysis for the Greater Alpine region: performance and expected future change. J Geophys Res Atmos 121:7710–7728

Solaymani HR, Gosain AK (2015) Assessment of climate change impacts in a semi-arid watershed in Iran using regional climate models. J Water Clim Change 6(1):161–180

Nakícenovíc N, Alcamo J, Davis G, de Vries B, Fenhann J, Gaffin S, Gregory K, Grübler A, Jung TY, Kram T, Emilio la Rovere E, Michaelis L, Mori S, Morita T, Pepper W, Pitcher H, Price L, Riahi K, Roehrl A, Rogner H-H, Sankovski A, Schlesinger ME, Shukla PR, Smith S, Swart RJ, van Rooyen S, Victor N, Dadi Z (2000) Special report on emissions scenarios. Cambridge University Press, Cambridge

Stocker TF, Qin D, Plattner G-K, Tignor M, Allen SK, Boschung J, Nauels A, Xia Y, Bex V, Midgley PM (eds) (2013) Climate change 2013: the physical science basis. Contribution of working group I to the fifth assessment report of the intergovernmental panel on climate change. Cambridge University Press, Cambridge, p 1535 IPCC

Taylor KE, Stouffer RJ, Meehl GA (2012) An overview of CMIP5 and the experiment design. Bull Am Meteorol Soc 93(4):485–498

Terink W, Immerzeel WW, Droogers P (2013) Climate change projections of precipitation and reference evapotranspiration for the Middle East and Northern Africa until 2050. Int J Climatol 33:3055–3072

Thornthwaite CW (1948) An approach toward a rational classification of climate. Geogr Rev 38:55–94

Van der Schrier G, Jones PD, Briffa KR (2011) The sensitivity of the PDSI to the Thornthwaite and Penman-Monteith parameterizations for potential evapotranspiration. J Geophys Res Atmos 116:D03106. https://doi.org/10.1029/2010JD015001

Webb RW, Rosenzweig CE, Levine ER (2000) Global soil texture and derived water-holding capacities from Oak ridge national laboratory distributed active archive center, Oak Ridge. http://www.daac.ornl.gov. Accessed 28 Feb 2018

Wells N, Goddard S, Hayes MJ (2004) A self-calibrating Palmer drought severity index. J Clim 17:2335–2351

Zareian MJ, Eslamain S, Safavi HR (2015) A modified regionalization weighting approach for climate change impact assessment at watershed scale. Theor Appl Climatol 122:497–516

Zittis G, Hadjinicolaou P, Lelieveld J (2014) Comparison of WRF model physics parameterizations over the MENA-CORDEX domain. Am J Clim Change 03(05):490–511